Master's thesis

NTNU
Norwegian University of Science and Technology
Faculty of Medicine and Health Sciences
Department of Clinical and Molecular Medicine

Martine Engebakken Berg

Generation and Characterization of Induced Pluripotent Stem Cells from Individuals Affected by Metachromatic Leukodystrophy

Master's thesis in Molecular Medicine
Supervisor: Barbara van Loon
Co-supervisor: Rabina Dumaru
May 2024

NTNU
Norwegian University of
Science and Technology

Martine Engebakken Berg

Generation and Characterization of Induced Pluripotent Stem Cells from Individuals Affected by Metachromatic Leukodystrophy

Master's thesis in Molecular Medicine
Supervisor: Barbara van Loon
Co-supervisor: Rabina Dumaru
May 2024

Norwegian University of Science and Technology
Faculty of Medicine and Health Sciences
Department of Clinical and Molecular Medicine

NTNU
Norwegian University of
Science and Technology

Acknowledgments

This thesis was written as part of the master's program in Molecular Medicine at the Norwegian University of Science and Technology (NTNU), Faculty of Medicine and Health Sciences. All research was conducted at the Department of Clinical and Molecular Medicine (IKOM), within the research group led by Barbara van Loon.

First and foremost, I would like to express my deepest gratitude to my supervisor, Barbara van Loon, for including me in her research group. Her guidance and support has been invaluable throughout my research journey. Her expertise and insights has greatly enriched my experience and contributed significantly to the completion of this thesis.

Special thanks to my co-supervisor, Rabina Dumaru, for her incredible support both in the lab and during the writing process. Her teaching and mentoring has been absolutely essential in developing my skills and knowledge in the lab. I am deeply grateful for her dedication throughout this past year.

I would also like to thank my other group members, Ezgi Aksu, Kayla Grooms and Kristin Rian. You have always been willing to help out, giving essential support and insights when needed. Additionally, I wish to thank all the lab members of IKOM who have been there to assist whenever I needed help.

Lastly, I would like to thank my family and friends for their tremendous support and encouragement throughout this process.

Abstract

Metachromatic leukodystrophy (MLD) is a devastating lysosomal storage disorder (LSD) caused by a deficiency in the enzyme arylsulfatase A (ARSA). This enzyme plays a crucial role in the degradation of sulfatides, which are central lipid components in the proper functioning of the myelin sheaths surrounding neurons. Without functional ARSA, sulfatides accumulate in the cells, thus leading to progressive demyelination. This impairs motor and cognitive skills and ultimately results in severe neurological decline. While the genetic basis of MLD and manifestation of the disease has been established, all molecular mechanisms leading to demyelination remain largely unknown.

The aim of this thesis was to establish a basis for investigating the pathomechanisms of MLD by generating and characterizing human induced pluripotent stem cells (hiPSCs) as patient-specific models. hiPSCs were obtained by reprograming peripheral blood mononuclear cells (PBMCs) from donors of an MLD-affected family consisting of a diseased child and healthy, carrier parents. Genome integrity, expression of proliferation, pluripotency and germ layer markers was assessed among the hiPSCs to evaluate hiPSC quality, and to compare characteristics between diseased- and healthy-derived hiPSCs.

hiPSCs were successfully generated from the three individuals. Comparable expression of pluripotency markers, OCT4, SSEA4, NANOG and SOX2, and proliferation marker Ki67 indicated a stable pluripotent state among the hiPSCs. Subsequent assessments of DNA damage levels in hiPSCs and germ layer marker expression across embryoid bodies (EBs) revealed varying levels among the individuals. Thus raising a question of how individual differences might affect hiPSC state and quality. However, limited sample size reduces the conclusiveness of these findings. Further studies are needed to elucidate the MLD-specific causes of disease and eliminate the impact of individually-derived differences.

Sammendrag

Metakromatisk leukodystrofi (MLD) er en ødeleggende lysosomal avleiringssykdom (LSD) forårsaket av mangel på enzymet arylsulfatase A (ARSA). Dette enzymet spiller en avgjørende rolle i nedbrytningen av sulfatider, som er sentrale lipidkomponenter som bidrar til korrekt funksjon av myelinskjedene rundt nervecellene. Uten funksjonell ARSA akkumulerer sulfatider i cellene, noe som fører til progressiv demyelinisering. Dette påvirker motoriske og kognitive ferdigheter, og resulterer til slutt i alvorlig nevrologisk nedbryting av nervesystemet. Selv om den genetiske bakgrunnen for MLD og etterfølgende sykdomsuttrykk er fastslått, er de molekylære mekanismer som fører til demyelinisering stort sett ukjente.

Målet med dette prosjektet var å etablere et grunnlag for å undersøke patomekanismene i MLD ved å generere og karakterisere menneskelige induserte pluripotente stamceller (hiPSC) som pasientspesifikke modeller. hiPSCs ble generert ved reprogrammering av perifere mononukleære celler (PBMCs) fra donorer i en MLD-rammet familie, bestående av et sykt barn, og friske foreldre som var bærere for sykdommen. Genom-integritet, uttrykk av proliferasjon-, pluripotens- og kimlagmarkører ble vurdert blant hiPSCs for å evaluere hiPSC-kvalitet, og sammenligne egenskaper i hiPSCs mellom barn med MLD og friske kontroller.

hiPSCs ble vellykket generert fra de tre individene. hiPSCs viste sammenlignbart uttrykk av pluripotensmarkører, OCT4, SSEA4, NANOG og SOX2, og proliferasjonsmarkør Ki67, noe som indikerer en stabil pluripotent tilstand. Videre vurdering av DNA-skade nivåer i hiPSCs og uttrykk av kimlagmarkører i embryoid bodies (EBs) viste varierende nivåer blant individene, noe som stiller spørsmålet om hvordan individuelle forskjeller kan påvirke hiPSC-tilstand og kvalitet. Imidlertid reduserer den begrensede prøvestørrelsen konklusjonen til disse funnene. Videre studier er nødvendige for å klarlegge de eksakte årsakene til MLD og eliminere innvirkningen av individuelle forskjeller.

Table of Contents

List of Figures

List of Tables

Abbreviations

ARSA	Arylsulfatase A
BBB	Blood-brain barrier
BMP4	Bone morphogenetic protein 4
cAMP	Cyclic AMP
CNS	Central nervous system
CSF	Cerebrospinal fluid
E8	Essential 8
EB	Embryoid body
EPR	Endoplasmic reticulum
ERT	Enzyme replacement therapy
FOXC1	Forkhead box C1
GalC	Galactosylceramide
GATA4	GATA binding protein 4
hiPSC	Human induced pluripotent stem cell
hPSC	Human pluripotent stem cell
HSC-GT	Hematopoietic stem cell gene therapy
HSCT	Hematopoietic stem cell transplantation
IF	Immunofluorescence
IL-1Ra	Interleukin-1 receptor antagonist
IL-8	Interleukin-8
iPSC	Induced pluripotent stem cell
LSD	Lysosomal storage disorder
M6P	Mannose-6-phosphate
MBP	Myelin basic protein
MCP-1	Monocyte chemoattractant protein-1
MIP-1β	Macrophage inflammatory protein-1 beta
MLD	Metachromatic leukodystrophy
MOI	Multiplicity of infection
MRI	Magnetic resonance imaging
MUT	Mutated

NANOG	Homeobox protein NANOG
NESTIN	Neuroepithelial stem cell protein
NPC	Neuroepithelial progenitor cell
O/N	Over night
O4	Surface antigen O4
OCT4	Octamer-binding transcription factor 4
OL	Oligodendrocyte
OLIG2	Oligodendrocyte transcription factor 2
OPC	Oligodendrocyte progenitor cell
P/S	Penicillin-Streptomycin
PAX6	Paired box protein 6
PBMC	Peripheral blood mononuclear cell
PBS-T	PBS-Tween 20
PFA	Paraformaldehyde
PLO	Poly-L-ornithine
PNS	Peripheral nervous system
ROCKi	Rho-kinase inhibitor Y-27632
ROS	Reactive oxygen species
RT	Room temperature
RT-qPCR	Reverse transcription-quantitative polymerase chain reaction
SapB	Sphingolipid activator protein B
SOX10	Sex determining region Y-box 10
SOX17	Sex determining region Y-box 17
SOX2	Sex determining region Y-box 2
SSEA4	Stage-specific embryonic antigen 4
TNFα	Tumor necrosis factor alpha
VEGF	Vascular endothelial growth factor
WT	Wild type

1. Introduction

1.1. Lysosomal storage disorders

Lysosomes are essential organelles within eukaryotic cells, serving as the primary site for the breakdown and recycling of macromolecules (1). These membrane-bound organelles are rich in hydrolytic enzymes, which are active at the acidic pH maintained within the lysosome (2). This unique environment allows for the efficient breakdown of various substances, including proteins, lipids, nucleic acids, and carbohydrates (1). Functional lysosomes are essential in several cellular processes as they are involved in the turnover of cellular components, enabling the cell to renew itself continuously. This process is vital for maintaining cellular health and function, allowing cells to rid themselves of damaged or obsolete components (3). In addition to the important role as the cell's recycling center, the lysosome can also contribute in retrieving information regarding changes in environmental conditions, such as nutrient availability, growth and stress signals (2). The hydrolytic enzymes are synthesized in the endoplasmic reticulum (EPR), processed as inactive pro-enzymes in the Golgi apparatus, and targeted to lysosomes by a mannose-6-phosphate (M6P) marker. This targeting mechanism is facilitated by the M6P receptor, which ensures that the enzymes are correctly delivered to the lysosomes (1). The proper functioning of lysosomes is critical, and disruptions in their processes can lead to severe consequences, as evidenced by the development of lysosomal storage disorders (LSDs) (4).

LSDs are metabolic diseases characterized by impaired degradation of macromolecules due to defective lysosomal function (2). The main consequence of LSDs is the accumulation of undegraded substances in various organs and tissues, which can interfere with molecular processes and have detrimental effects on cellular function (Figure 1.1) (2). Around 70 LSDs have been identified so far, and it is anticipated that this number will grow as ongoing research and advances in genetic testing uncover more disorders (5). The prevalence of LSDs ranges between 1:57000 and 1:4200000 individuals (6). However, when considered collectively, it is estimated that LSDs may impact as many as 1 in 5000 live births (6). Therefore, despite each individual LSD usually being rare, the collective prevalence of LSDs constitutes a great proportion of genetic metabolic disorders (5). When combined with the ongoing absence of completely successful

therapies for numerous LSDs, these diseases frequently result in a high rate of disease-related complications and premature death (7).

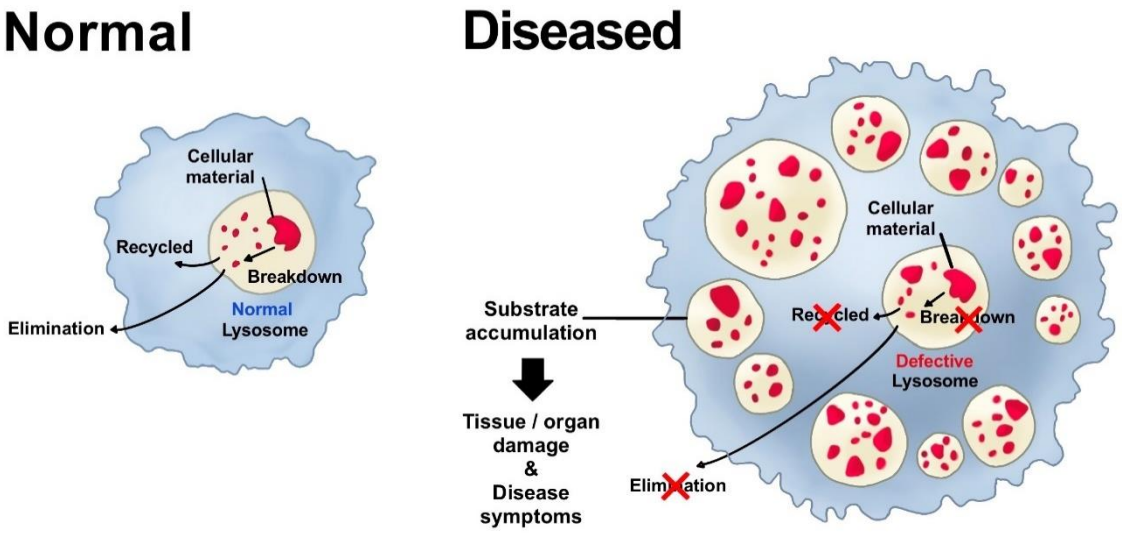

Figure 1.1. Lysosomal function in normal and diseased states.
In normal lysosomal function, cellular material is degraded and subsequently either recycled or eliminated as waste material, maintaining cellular homeostasis and function. In diseased cells impacted by LSDs, substrates accumulate due to the inability of lysosomes to sufficiently break down cellular material. Substrate buildup leads to lysosomal enlargement and dysfunction, which consequently causes tissue and organ damage, culminating in the clinical symptoms associated with LSDs. Figure adapted from Avrobio.com (8).

The majority of LSDs are caused by genetic mutations in enzyme- or protein-encoding genes related to lysosomal function, and follows an autosomal, recessive inheritance pattern (2). The classification of LSDs is based on the primary substrate that accumulates in the given disease, and are broadly categorized into mucopolysaccharidoses, mucolipidoses, glycoproteinoses, sphingolipidoses, oligosaccharidosis and glycogen storage diseases (Table 1.1) (1). The class of sphingolipidosis, in particular, is characterized by the accumulation of complex sphingosine lipids containing phospholipids (5). Diseases within the class of sphingolipidosis involve the production of a mutant enzyme that is unable to efficiently degrade sphingolipids (9). The phenotypic outcome in patients can be largely varied. Some patients may show no symptoms or only mild, unrecognized signs of the disease. Others can experience severe, rapidly progressing forms of the disease that affect the nervous system, which can be fatal. Even within the same disease, the presentation can differ significantly. Some patients develop symptoms early in life, while others may not show signs until later in adulthood (7).

Table 1.1. Classification and examples of common LSDs.

Disease	Defective Protein	Primary Storage Material	OMIM
	Sphingolipidoses (9)		
Fabry disease	α-galactosidase A	Galactosylated glycoplipids	301500
Gaucher disease, type I, II and III	β-glucosidase	Glucosylceramide	230800, 230900, 231000
Niemann-Pick	Sphingomyelinase	Sphingomyelin	257220
Metachromatic Leukodystrophy	Arylsulfatase A, Saposin B	Sulfatide	250100
	Mucopolysaccharidoses (10)		
MPS I (Hurler)	α-Iduronidase	Dermatan and heparan sulfate	607014
MPS II (Hunter)	Iduronate-2-sulphatase	Dermatan and heparan sulfate	309900
	Mucolipidoses (11)		
ML type II (I-cell disease)	UDP-N-acetylglucoseamine-1-phosphotransferase	Cholesterol, phospholipids, glycosaminoglycans	252500
	Glycogen storage diseases (12)		
Pompe disease	α-Glucosidase	Glycogen	232300
	Glycoproteinoses (13)		
Fucosidosis	α-L-fucosidase	Glycoproteins, glycolipids	230000
	Oligosaccharidosis (14, 15)		
Mannosidosis, type α and β	α-mannosidase β-mannosidase	Mannose-oligosaccharides	248500, 248510

1.2. Metachromatic leukodystrophy

Within the spectrum of LSDs, metachromatic leukodystrophy (MLD) emerges as an illustrative example of how these disorders specifically affect the nervous system. MLD belongs to the class of sphingolipidosis, that is characterized by the accumulation of complex sphingosine lipids containing phospholipids (5). As is the case for most LSDs, MLD follows an autosomal recessive inheritance pattern, meaning that the affected individual must inherit two copies of the faulty gene, one from each parent (16). As the name implies, MLD belongs to the group of leukodystrophies, where MLD is amongst the most common (17). Leukodystrophies are characterized by the progressive degeneration of the white matter in the brain, and are classified based on magnetic resonance imaging (MRI) appearance, cellular pathophysiology, metabolic and molecular

mechanisms (18). The term “white matter” arises from the appearance of myelin, which is rich in lipids and thus has a fatty, white appearance (19). MLD has also gotten its name due to the distinctive presence of metachromatic granules within the affected cells. These granules are formed due to the accumulation of sulfatides, where “metachromatic" refers to the color-changing property of these granules when stained and observed under a microscope (20). This unique staining characteristic is indicative of the disease's pathology, where the accumulation of these substances disrupts normal myelin structure and function (20).

1.2.1. Genetic background

MLD is primarily caused by mutations in the *ARSA* gene (OMIM 250100), but can also in certain cases be caused by mutations in the *PSAP* gene (OMIM 249900) (21). *ARSA* is located on chromosome 22q13.31-qter and consists of eight exons (NCBI Reference Sequence NG_009260.2). To date, 282 unique mutations have been described for *ARSA*, thus making this gene the most commonly mutated in MLD patients (Figure 1.2) (22).

PSAP, on the other hand, is located on chromosome 10q21-q22 and consists of 14 exons (NCBI Reference Sequence NG_009301.1). 84 unique variants have been reported so far for the *PSAP* gene (23). While being less common, mutations in *PSAP* result in the classical MLD phenotype, similar to *ARSA* mutations (21). The *ARSA* gene encodes for arylsulfatase A (ARSA) enzyme, whereas *PSAP* encodes the sphingolipid activator protein B (SapB) (21). ARSA is classified as a sulfatase enzyme, which is essential in the breakdown of sulfatides in the lysosomes. Functional ARSA enzyme carry out the cleavage reaction of sulfatides, only when making a complex with SapB, which presents the sulfatide to the active site of ARSA. Only 10-15% of ARSA enzymatic activity is necessary for the normal degradation of sulfatides. However, there are no other compensatory enzymes that can redeem a total deficiency (21). Loss of either of these enzymes can therefore induce severe symptoms, and lead to the development of the different subtypes of MLD.

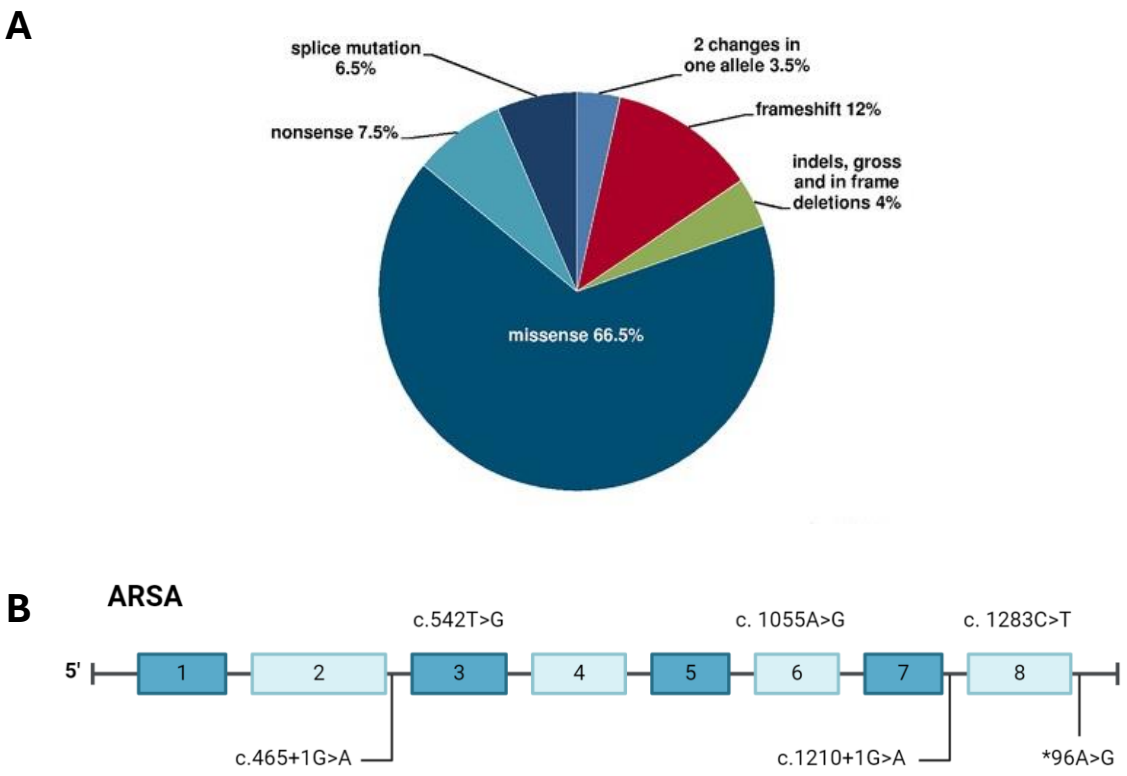

Figure 1.2. Schematic representation of *ARSA* gene and the common mutations identified in MLD.
A. Percentage distribution of different types of genetic mutations found in the *ARSA* gene. Figure adopted from Cesani et al. 2016 (24). **B.** Graphical representation of the *ARSA* gene, composed of eight exons (boxes numbered 1-8) and introns (grey lines between exons). Highlighted within the gene are the locations of the most common mutations associated with MLD: splice site mutations (c.465+1G>A and c.1210+1G>A), missense mutations (c.1283C>T and c.542T>G) and pseudodeficiency alleles (c.1055A>G and ∗96A>G). Figure created in Biorender.com.

1.3. Clinical manifestation

Three main classifications of MLD have been characterized based on the age of onset and rate of disease progression (25). These three forms are the late-infantile, juvenile, and adult forms, and symptoms and functional deterioration can vary between the subtypes (Table 1.2) (20). Lower levels of ARSA enzyme activity typically coincide with an earlier age of onset, a more aggressive progression of disease and an expected lifespan. However, a direct link between the severity of the disease and the levels of remaining ARSA activity has not been conclusively determined (26). Despite the variability in the onset and progression rate among the different forms of MLD, the disease invariably leads to a decline in quality of life, ultimately ending in a vegetative state and premature death (20).

Table 1.2. Comparative characteristics of MLD subtypes.

	Late-infantile	Juvenile		Adult
		Early-juvenile	Late-juvenile	
ARSA Activity (27)	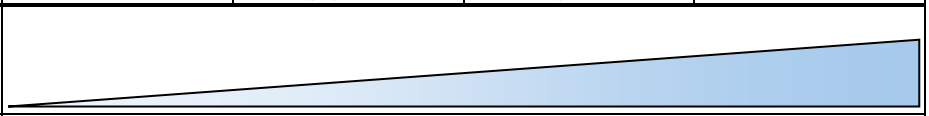			
Genotype (27)	0/0	0/R		R/R
Age of Onset (26, 28, 29)	< 30 months	30 months to < 6 years	6 years to <16 years	> 16 years
Occurrence (21, 29)	50-60%	20-30%		15-20%
Disease Progression (21, 29)	Rapid	Variable		Slow

1.3.1. Genotype-phenotype correlation

Typically, the age at which symptoms first appear is indicative of the specific type of MLD a patient may have. However, the correlation can vary widely, with different onset ages even among members of the same family with the same mutation (21). Disease-causing mutations of MLD are distinguished into 2 forms: "null alleles (0-alleles)" resulting in complete loss of enzymatic activity, and "R-alleles" which encodes enzyme with some residual enzyme activity (16). Although difficult to establish an exact relationship between mutation and phenotypic consequence, there is a general consensus that having two 0-alleles results in late-infantile MLD, genotypes heterozygous for 0- and R-alleles cause juvenile MLD, and two copies of an R-allele gives the adult form of MLD (16). The predictive value of the phenotype based on genetic mutation is most effective for patients homozygous for 0-alleles, while individuals with one or two R-allele copies show more variability between phenotypic outcome (30).

The majority of affected alleles in MLD have single-point mutations with the most common being missense mutations accounting for around 66.5% of described mutations (24). Following this, 7.5% are considered nonsense mutations, and 6.5% affect splice sites, and a combined total of 12% of the affected *ARSA* alleles are due to deletions, insertions, duplications, and inversions that cause frame shifts (Figure 1.2 A) (24). The most common pathogenic *ARSA* variants are caused by mutations in the splice donor sites,

such as c.465+1G>A and c.1210+1G>A, which are 0-alleles and frequently present in late-infantile patients where they occur either as homozygous or compound heterozygous mutations (Figure 1.2 B) (26, 30). Other common disease variants are the missense mutations c.1283C>T and c.542T>G typically associated with juvenile and adult forms of MLD (24).

In addition to disease-causing allelic variants, *ARSA* variants can also include "*ARSA* pseudodeficiency alleles (Pd-alleles)" (25). This allele type was identified in seemingly healthy individuals, where ARSA activity has been measured to be low without the manifestation of MLD (31). ARSA activity in individuals with pseudodeficiency mutations is sufficient for a normal phenotype and turnover of sulfatides to prevent clinical manifestation, even when appearing as homozygous mutations (24, 31). Common Pd-alleles include c.1055A>G transition modifying a glycosylation site and ∗96A>G transition, which affects the main *ARSA* mRNA form, both leading to reduced enzyme activity (24).

1.3.2. MLD subtypes

The late-infantile form of MLD is the most common disease type, and constitutes for 50-60% of all MLD patients (29). In this form of the disease, symptoms usually manifest before 30 months of age (26). The late-infantile form is characterized by a rapid disease progression, often after a period where development seems to proceed normally (20). Initial symptoms are often recognized as a lack of developmental milestones, gait abnormalities and loss of muscle strength (20). As the disease advances, more adverse symptoms are observed, such as regression of speech, dysphagia, spasticity, swallowing difficulties, loss of cognitive and motor abilities as well as visual and hearing impairment. Later stages include severe regression in psychomotor skills, seizures and spasms, leading to a vegetative stage with feeding and respiratory problems (21). Death occurs in childhood, usually a few years after disease onset, and is thus considered the most severe form of MLD (21).

The juvenile form of MLD is usually divided into subgroups: early-juvenile with a disease onset between 2.6 years to 6 years, and late-juvenile form with an onset ranging between 6 to 16 years (28). Around 20-30% of MLD patients are diagnosed with the juvenile form,

and clinical symptoms can vary highly between individuals (21). However, symptoms in the juvenile form are, in general, thought to be less pronounced than in the late-infantile form (21). In the juvenile form, the disease typically initiates with noticeable behavioral changes and psychiatric symptoms, alongside a delay in developing fine motor skills and issues with attention and concentration, reflecting early cognitive impairment (20). Challenges with learning and concentration impairment are frequently observed as part of the early symptoms (32). As the condition progresses, motor skills begin to deteriorate, and similar to late-infantile form, are being accompanied by muscle stiffness, spastic movements, and abnormal posturing, marking a decline in both central and peripheral motility (21, 32). The progression of MLD in the juvenile stage, especially in the early-juvenile, is rapid, leading to a significantly reduced lifespan in the absence of therapeutic intervention. Implementation of supportive treatments, such as gastrostomy for nutritional support and antibiotics to manage infections, can extend the lives of affected individuals, though they may ultimately enter a vegetative state (21).

The adult form of MLD, accounts for approximately 15-20% of all MLD cases, making it the least common form (21). This form is known to present with a more variable and often later onset, typically occurring after 16 years of age (29). Unlike the more aggressive late-infantile and juvenile forms, adult MLD often manifests with psychiatric symptoms and behavioral changes, such as sudden emotional changes, hallucinations, memory loss or depression (33). Because of this, adult form of MLD can often be mistaken for other mental health disorders, such as schizophrenia or early-onset dementia (34). Cognitive decline and motor dysfunction, such as ataxia and peripheral neuropathy, develop as the disease progresses, but at a slower rate compared to earlier-onset forms (21). Unlike the late-infantile form, where rapid progression leads to early mortality, the progression in the adult form can span several years to decades. However, the ultimate stages of the disease are similar to the forms with earlier onset (30).

1.4. Functional roles of ARSA and SapB

1.4.1. Sulfatide metabolism

To understand the impacts that *ARSA* mutations have on the onset of MLD, an understanding of sulfatide metabolism is needed. Sulfatides are a subgroup of glycosphingolipids located in the cell membrane that are central in physiological processes and responses (35). Biosynthesis of sulfatides begins in the EPR with the formation of ceramide, which is the precursor for all glycosphingolipids (Figure 1.3) (36). Ceramide can be formed through different pathways, including *de novo* synthesis, degradation of sphingomyelin or recycling of glycosphingolipids (36). Once ceramide has been synthesized, galactose is transferred to ceramide, resulting in the formation of galactosylceramide (GalC) (35). GalC is then transferred to the Golgi complex, where a sulfate group is added to the glycosphingolipid, forming a sulfatide molecule (35). Similar to all sphingolipids, sulfatides are characterized by structural diversity due to variations in the acyl chain lengths, which can undergo hydroxylation (35). The C24:1-sulfatide is the most abundant sulfatide in myelin, while shorter-chain fatty acid sulfatides, such as C18:0-sulfatide, are found at higher concentrations in cortical grey matter (35, 37).

Degradation of sulfatides is critical for maintaining cellular homeostasis and the proper functioning of the nervous system, particularly in the turnover and recycling of the myelin sheath components (38). Breakdown of sulfatides begins in the lysosomes, where the sulfate groups attached to the sulfatide are cleaved off in a hydrolysis reaction performed by ARSA (Figure 1.3) (35). This reaction transforms sulfatide into GalC, which is a less complex molecule that can be further broken down or reincorporated into the cell's membrane structures (35). The efficient degradation of sulfatides by ARSA is heavily dependent on the presence of SapB, the activator protein that enhances the interaction between sulfatides and ARSA. SapB plays a crucial role in extracting sulfatides from the lysosomal membrane, making them accessible to the active site of ARSA. As evident from MLD genotype presentation, the disruptions in this process lead to sulfatide accumulation, which in turn has detrimental effects on the structural integrity and function of the myelin sheath (36).

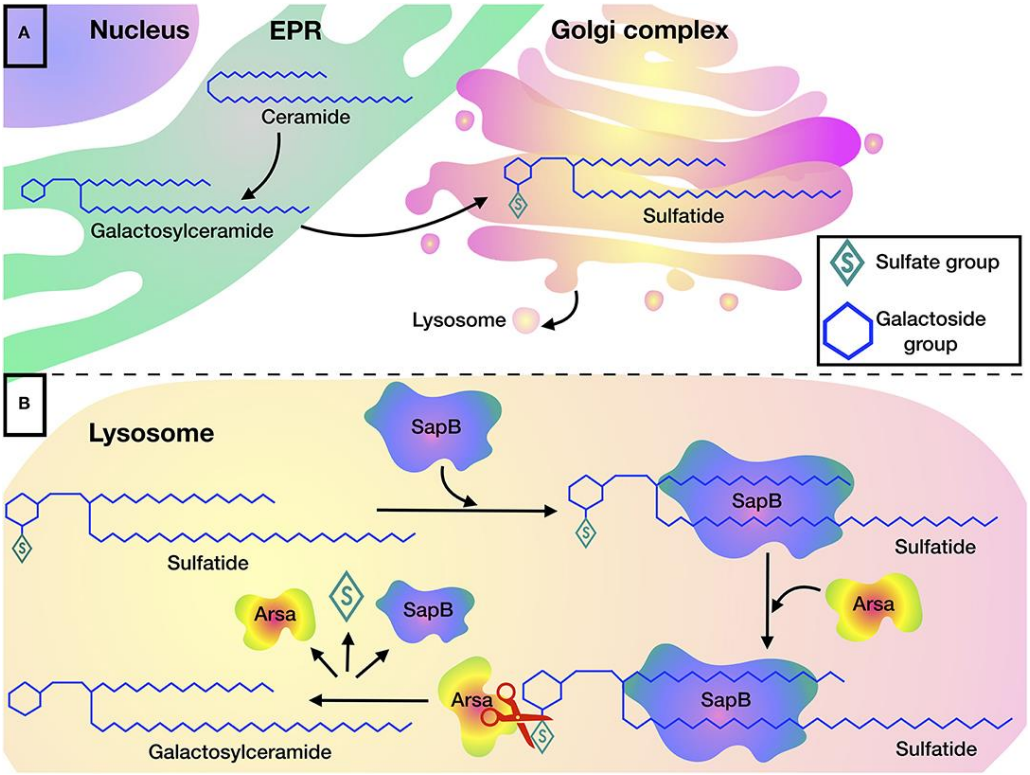

Figure 1.3. The role of ARSA and SapB in sulfatide metabolism.
A. The production of sulfatides begins in the endoplasmic reticulum (EPR), where the molecule galactosylceramide (GalC) is synthesized by the enzymatic transfer of galactose to ceramide. Following synthesis, galactosylceramide is transported to the Golgi apparatus, where it undergoes sulfation, gaining a sulfate group to become sulfatide. **B.** Sulfatide degradation occurs within the lysosome, where saposin B (SapB) is essential for presenting sulfatide to the active site of arylsulfatase A (ARSA). ARSA catalyzes the removal of the sulfate group from sulfatide, converting it back to galactosylceramide. Figure adopted from Shaimardanova et al. 2020 (21).

1.4.2. Myelination and its deregulation through sulfatide accumulation

In relation to the nervous system, sulfatides constitute around 4-6% of the lipids in the myelin sheath (35). Together with the sulfatide precursor, GalC, they make up one third of myelin lipids (35). The myelin sheath is crucial for effective nerve signaling, axon potential and protection of nerve fibers (39). Sulfatides are essential in the structural stability and proper functioning of myelinated nerve fibers, such as oligodendrocytes and Schwann cells (21). Additionally, sulfatides have also been found to be present in neurons and astrocytes in the grey matter of the brain (36).

Oligodendrocytes are the primary myelinating cells in the central nervous system (CNS), accounting for 5-10% of total glial population and ensuring rapid and efficient electrical

signal transmission along axons and preserving axonal integrity (40). Oligodendrocytes originate from oligodendrocyte progenitor cells (OPCs) that undergo a highly regulated differentiation process, which is critical for the timely production of myelin (40). The oligodendrocyte transcription factor 2 (OLIG2) is crucial in the differentiation of neuroepithelial progenitor cells (NPCs) to OPCs and is an indicator of oligodendrocyte-specific lineage (39). As the cells reach OPC stage, the oligodendrocyte marker 4 (O4) can be used to identify immature oligodendrocytes (39). Further oligodendrocyte development from OPCs involves a sequence of steps, from OPC proliferation to migration, adhesion to axons, synthesis of myelin components, and the wrapping and compaction of the myelin sheath around axons (39).

The oligodendrocyte differentiation process is regulated by several lipids and proteins, such as cholesterol, GalC and sulfatides (36). During embryonic development, OPCs eventually populate white matter tracts, initiating the myelination process (41). As differentiation advances, OPCs gradually lose their ability to migrate and proliferate, taking on a more complex morphology forming premyelinating oligodendrocytes (42). Mature oligodendrocytes can be validated by the presence of myelin basic protein (MBP), which is essential in myelination (39).

Sulfatides have been seen to be upregulated in early OPCs, before the cells begin to enclose neuronal axons with myelin fibers (36). Production of myelin is especially prominent in early childhood, starting postnatally around the age of three to four months (36). During this time, oligodendrocytes and Schwann cells rapidly generate large quantities of lipids, and the majority of myelination is completed around the age of two as observed through MRI (19, 36). Although white matter volume increases into adulthood, the pace slows down considerably, underlining the importance of correct myelin formation in early stages of development (19, 35).

In order to obtain proper myelination, oligodendrocytes have a high metabolic rate, which renders oligodendrocytes particularly susceptible to a variety of damage pathways (40). This can be triggered by the activation of several intracellular processes, often initiated by extracellular factors secreted by other cells within the CNS (40). This vulnerability can be especially relevant in the context of sulfatide accumulation, leading to the disruption of normal biochemical processes. In MLD, the sulfatide buildup results in demyelination, compromising the electrical insulation necessary for the efficient

transmission of neural signals (Figure 1.4), ultimately leading to several motor and cognitive impairments (43, 44). Although the exact relation between sulfatide accumulation and subsequent demyelination in MLD has not been determined, several potential pathways have been suggested.

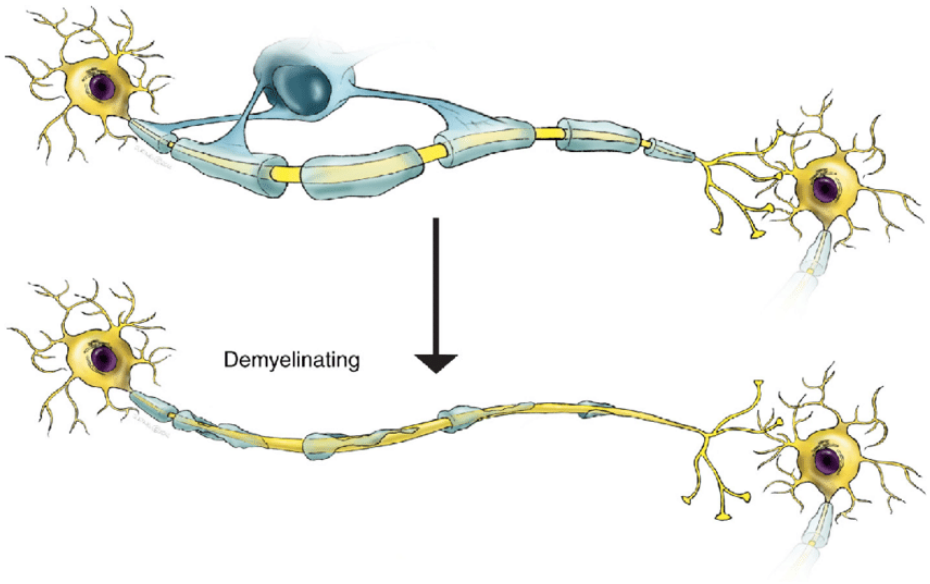

Figure 1.4. Impact of demyelination on neural conduction.
Under normal conditions, axons are extensively myelinated, allowing for efficient nerve signaling transmission through action potentials between neurons and ensuring the integrity of synaptic connections. Demyelination disrupts this process by damaging the myelin sheath, resulting in a significant loss of functional conduction. Destruction of myelin leads to the deterioration of synaptic connections and causes axonal damage. Figure adopted from Miller et al. 2017 (45).

OPCs and oligodendrocytes are particularly sensitive to oxidative stress, as they are characterized by low antioxidant levels. Thus limiting their capacity to neutralize harmful oxidative agents (39). Myelinating oligodendrocytes are especially vulnerable to damaging by-products, such as reactive oxygen species (ROS) and hydrogen peroxide, due to their high metabolic turnover (39, 46). Oligodendrocytes contain high levels of iron, which can react with hydrogen peroxide to produce reactive radicals (39). Increased oxidative stress can therefore be a contributing factor in oligodendrocyte damage, and subsequent demyelination.

Studies indicate that inflammation can contribute to MLD pathophysiology, as elevated levels of certain cytokines have been observed in the cerebrospinal fluid (CSF) and plasma of patients (47). Significantly elevated levels of monocyte chemoattractant protein-1 (MCP-1), interleukin-1 receptor antagonist (IL-1Ra), interleukin-8 (IL-8),

macrophage inflammatory protein-1 beta (MIP-1β), and vascular endothelial growth factor (VEGF) were found in MLD patients compared to healthy controls (47). The increased levels in MLD patients suggest a contribution to both the disease's neuropathological features and its systemic manifestation, which may be the result of sulfatide accumulation and neuronal damage (47). Other findings have shown that sulfatide increases cytosolic free calcium in neutrophils, and subsequent expression of mRNA for IL-8 and tumor necrosis factor alpha (TNFα) (48). Release of calcium into the cytosol can lead to activation of several stress-related pathways of the EPR, and influx of calcium into mitochondria (49). This has been found to cause permeabilization of the mitochondrial membrane, thus triggering the release of pro-apoptotic factors that contribute to driving the cell towards apoptosis (49).

Sulfatide accumulation is also thought to affect the immune response in the peripheral nervous system (PNS). Disease manifestation in the CNS has often been found to not correlate with the severity of neuropathy observed in the PNS (50). As CNS symptoms are the most noticeable in rapidly progressing MLD, data regarding the effects of peripheral neuropathy on MLD can often be limited (50). The lack of correlation between demyelination and the presence of metachromatic material found in peripheral nerves indicates that other factors, such as neuroinflammation, play a role in the pathology of peripheral neuropathy in MLD (50). It has been hypothesized that sulfatide accumulation leads to cell death in Schwann cells and macrophages, activating the complement pathway, thus targeting myelin for destruction. Subsequently, cytokines are released and recruit lymphocytes leading to further deterioration of the myelin sheath (50).

Microglia, the immune cells of the nervous system, have also been found to change immune phenotypes and exhibit early and severe damage in the pathogenesis of MLD. This damage precedes the major myelin breakdown observed in MLD, along with lysosomal breakdown and cell membrane lysis before significant oligodendrocyte damage and reduction in myelin density. The findings from the study by Bergner et al. indicate that as sulfatides accumulate in oligodendrocytes, defective myelin is taken up by microglia as an initial response to remove toxic substances and protect surrounding tissue. This eventually leads to microglia damage and aggravation of myelin deterioration (51).

1.5. Modeling MLD

1.5.1. Animal models

To better understand the pathogenesis of MLD, it is critical to find effective study models that recapitulate disease progression. No naturally occurring animals with MLD have been described, which has led to the generation of genetically modified mice to study the disease (52). Arsa-deficient mice (*Arsa*$^{-/-}$) were generated by homologous recombination showing no enzyme-activity, thus resembling the late-infantile form of MLD (52). Pathological features observed in humans were also seen in *Arsa*$^{-/-}$ mice, such as sulfatide accumulation and increased astrocyte activation. The *Arsa*$^{-/-}$ mice had symptoms of delayed brainstem auditory-evoked responses, ataxia, tremors, and weak muscle tone, which mimic the early manifestations of MLD in humans (52). However, the disease progression in mice does not advance to the severe demyelination, associated symptoms and shortened lifespan that characterize the human condition, suggesting that these mice might represent an initial phase of MLD (52). The buildup of sulfatide is a gradual process, requiring several months to reach levels that contribute to disease onset. Therefore the relatively brief lifespan of mice presents a challenge for accumulating sufficient levels of sulfatide to induce disease-related symptoms (53).

As myelin abnormalities were not observed in the *Arsa*$^{-/-}$ mouse model, a more accurate model was proposed by enhancing sulfatide synthesis. This was done by overexpressing the *Gal3st1* gene, involved in sulfatide synthesis, specifically in oligodendrocytes and Schwann cells (53). The transgenic *Arsa*$^{-/-}$ mice showed increased sulfatide and significant neurological symptoms and myelin pathology, similar to human MLD. This increase led to severe neurological symptoms, characterized by reduced nerve conduction velocity and peripheral neuropathy with hypomyelinated and demyelinated axons (53). The degree of demyelination was less pronounced in the CNS compared to the PNS. However, it was the first mouse model to accurately represent the myelin pathology seen in human cases of the disease (44). This mouse model has been used to test various treatments of MLD, such as gene integration using viral vectors (adeno-associated viral, lentiviral, and retroviral vectors), hematopoietic stem cell transplantation (HSCT) and intracerebral injection of recombinant ARSA (20). As differences between mouse models and human disease progression have been observed, this highlights the inherent

limitations of mouse models in fully recapitulating the human disease state, emphasizing the need for models that more closely reflect human biology.

1.5.2. iPSCs as study model for MLD

Recently, induced pluripotent stem cells (iPSCs) have emerged as a more appropriate model for studying human pathologies. iPSCs are derived from somatic cells, such as fibroblasts and peripheral blood mononuclear cells (PBMCs), and are subsequently reprogrammed back to a pluripotent state by introducing specific sets of transcription factors, such as Octamer-binding factor 3/4 (OCT3/4), sex determining region Y-box 2 (SOX2), Krüppel-like factor 4 (KLF4), and cellular MYC (c-MYC) (54). iPSCs have several distinctive characteristics ensuring their pluripotency, ability of self-renewal as well as the potential to differentiate into other cell types. To validate their undifferentiated state, iPSC should express specific pluripotency markers such as the transcription factors OCT4, SOX2 and Nanog homeobox (NANOG) (55). Additionally, surface markers like stage-specific embryonic antigen-4 (SSEA4), are commonly used to identify iPSCs (56). Functional criteria of iPSCs include the ability to form chimeras through injection into early-stage embryos, as well as teratoma formation, demonstrating their ability to contribute to various embryonic and extraembryonic tissues (55). Embryoid body (EB) formation is another method for assessing the pluripotency of iPSCs. EBs are three-dimensional (3D) aggregates of stem cells that have the ability to differentiate spontaneously into cell types from all three germ layers: endoderm, mesoderm, and ectoderm (Figure 1.5) (57). Thus, the ability of iPSCs to form EBs can be used as a method to demonstrate their pluripotency *in vitro,* and further differentiation potential.

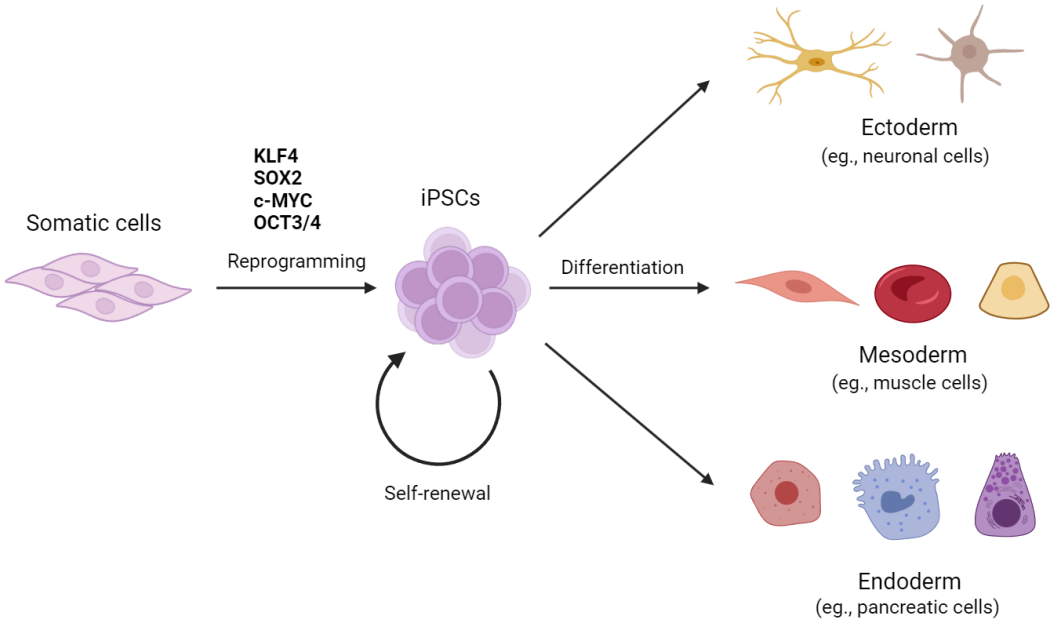

Figure 1.5. Generation of iPSCs from somatic cells and subsequent differentiation into cell types from the three germ layers.
Process of reprogramming somatic cells to generate iPSCs. Starting with the collection of somatic cells (e.g., PBMCs or skin fibroblasts), these cells undergo genetic reprogramming through the introduction of specific transcription factors, leading to the formation of iPSCs. iPSCs are characterized by their ability to self-renew and maintain pluripotency. Additionally, iPSCs can undergo differentiation into the three germ layers: ectoderm, mesoderm, and endoderm (e.g., neurons for ectoderm, muscle cells for mesoderm, and pancreatic cells for endoderm). Figure created in BioRender.

Expression of different markers can be analyzed to assess the developmental progression and differentiation status of EBs. Endodermal markers include GATA-binding protein-4 (GATA4) and sex determining region Y-box 17 (SOX17), which are involved in the development of the gastrointestinal, respiratory, and urinary systems, along with various endocrine glands (58). Forkhead box C1 (FOXC1) and bone morphogenetic protein 4 (BMP4) are examples of mesodermal markers contributing to the development of structures such as the notochord, skeletal and smooth muscle, cartilage and connective tissues, as well as forming kidneys and blood cells (58). Markers for the ectoderm are neuroepithelial stem cell protein (NESTIN) and paired box 6 (PAX6), indicating development into various components of the nervous system (58). By analyzing these markers within EBs, differentiation potential of iPSCs can be validated, and allow for further differentiation towards different cell types. This ability makes iPSCs especially versatile for studying a wide array of diseases.

iPSCs have been used in a few studies previously to determine the pathological events in MLD, by conducting differentiation of iPSCs to various neural cell types, including NPCs, mature neurons, astrocytes, and oligodendrocytes (59, 60). A study by Doerr et al. generated iPSCs from a juvenile MLD patient using retroviral methods to introduce reprogramming factors (60). The iPSCs were then differentiated into two types of neural cells: long-term self-renewing neuroepithelial stem cells and astroglial progenitors. These cells were specifically engineered to overexpress ARSA with the aim to replace deficient enzyme in MLD patients. To evaluate the therapeutic potential of these engineered cells, they were transplanted into the brain of Arsa-deficient mice, which resulted in a significant reduction in sulfatide accumulation in the brain tissues of these mice. This indicates that the transplanted cells successfully compensated for the enzyme deficiency and mitigated the biochemical pathology associated with MLD (60).

Another study by Frati et al. demonstrated the generation of iPSCs from two MLD patients and further differentiation into NPCs (59). iPSCs were differentiated into mature neurons, astrocytes, and oligodendrocytes, where significant sulfatide accumulation and alterations in sulfatide composition were observed. Differentiation of NPCs to neuronal and glial cells was found to be impaired, as cells showed reduced levels of markers for oligodendroglia and astroglia, in addition to reduced numbers of neurons and organized neuronal networks. Secondary pathological events such as lysosomal compartment expansion, oxidative stress, and enhanced apoptosis rates were also observed. It has been further demonstrated that restoring functional ARSA enzyme levels in MLD cells, via lentiviral-mediated gene transfer, could normalize sulfatide levels and compositions (59). This demonstrates how the pathological phenotype can be rescued by ARSA reconstitution and underscores the potential of using iPSCs to provide new understanding of MLD disease mechanisms.

While conventional 2D cell cultures have provided valuable insights, it is crucial to recognize that neurodevelopment and disease progression occur within a 3D microenvironment (61). This underscores the necessity for advanced 3D models to comprehensively study neurodevelopment and neurodegenerative diseases such MLD. Such 3D models include spheroids and organoids that more accurately represent the organization of brain tissue, which is particularly relevant for MLD research (61). Organoids arise from stem cells or organ-specific progenitor cells and develop through

self-organization processes that mimic the structure of an organ, and can exhibit some of the key characteristics and functions of the target tissue (62).

The use of 3D organoid models can be particularly valuable when using MLD-patient-specific human induced pluripotent stem cells (hiPSCs) for organoid formation, as this allows for the study of myelination and demyelination processes in a more physiologically relevant context (62). The use of cerebral organoids have been used in the study of other neurodegenerative diseases such as Alzheimer's disease, where they have contributed to elucidate elements of the underlying pathophysiology (63). Similarly, for MLD, organoids could model the impact of ARSA deficiency and sulfatide accumulations that characterize the disease in a more accurate environment compared to 2D *in vitro* models.

1.5.3. *In silico*-based models

Advancements within computational technologies allow for the development of *in silico*-based methods to study disease modeling and potential drug targets of MLD. Computational modeling can provide valuable insight into molecular mechanisms by simulating the interactions between enzymes and substrates for instance, to explore therapeutic targets (64).

In silico models enable the screening of large compound libraries for potential drug candidates, and can be used in the optimization of already existing treatment strategies or in the discovery of other possibilities. Integration of computational simulations with biological insights can also be used to create detailed models of brain organoids that represent the pathophysiological environment of MLD. A study by Esmail et al. utilized simulations to provide insights into the molecular mechanisms of lysosomal dysfunction and identified affected kinase pathways, guiding drug repurposing efforts for MLD treatment. Such approaches can reveal the intricate details regarding enzyme deficiencies, accumulation of sulfatides, and their deleterious effects on neural cells and myelin sheaths. This allows for a high-throughput screening of genetic mutations and their phenotypic manifestations, and the ability to simulate various disease states within a controlled virtual environment (65).

1.6. Current treatment options for MLD

In all three MLD forms, the disease is progressive and ultimately fatal. Due to still rather limited knowledge regarding the pathomechanisms behind the disease and technical limitations, few treatment options are available. Until recently, there has been no effective treatment for the disease, and especially for the early-onset forms, the main treatment option has been palliative care (66). Such supportive care includes medication to relieve pain and muscle spasms, nutritional support as well as physical therapy to preserve muscle function and flexibility for as long as possible to enhance life quality (67, 68). As MLD is a neurodegenerative disease affecting the central and peripheral nervous system, one of the main issues in developing effective treatment is overcoming the permeability of the blood-brain barrier (BBB) to systematically deliver therapeutic drugs (69). However, some treatment options are available and under development, potentially altering the course of the disease especially when applied early in progression.

In treatment of MLD, the aim is to restore ARSA levels, increasing the degradation of sulfatides to inhibit neurodegeneration. One of the proposed medical treatments for MLD is enzyme replacement therapy (ERT). The goal with such treatments is to replace the non-functional enzymes in the patient, by intravenous infusion to increase enzyme levels (70). ERT has been effective in the treatment of other LSDs and has led to stabilization and enhancement of somatic symptoms (70). However, these improvements are primarily seen in LSDs without involvement of the CNS, which is not the case for MLD (69). Studies with MLD mouse models demonstrated that recombinant ARSA enzyme infusion reduced sulfatide storage in peripheral nerves and in the CNS, with improved MLD symptoms at early treatment (71). To overcome the BBB, intrathecal infusion of enzyme directly into the CSF has been a proposed treatment, where sulfatide levels were found to decrease in *Arsa*$^{-/-}$ (69, 72).

Given that bone marrow-derived monocytic cells are able to cross the BBB, allogeneic HSCT has emerged as a viable treatment option for MLD to replenish enzyme activity within affected cells (69, 73). Monocytic cells enter the CNS and transform into microglial cells that produce ARSA enzyme, which subsequently is secreted and absorbed by oligodendrocytes and neurons (74). However, the process of replacing native microglia is slow, and progression of neuropathology in patients continues before reaching adequate levels of ARSA enzyme (69). Consequently, HSCT is not effective for

rapid progression or advanced symptoms of MLD, and is only used in non- or presymptomatic MLD cases (75).

The absence of effective therapies for many individuals with MLD, especially early-onset variants, has driven the advancement of *ex vivo* gene therapy as a novel therapeutic strategy. Autologous CD34+ hematopoietic stem cells are extracted from a patient's bone marrow or peripheral blood and transduced *in vitro* with a lentiviral vector containing a functional copy of *ARSA*, before infusion back to the patient where cells engraft in the bone marrow and produce functional ARSA at supranormal levels (Figure 1.6) (18, 69). Studies in mouse models initially demonstrated that hematopoietic stem cell gene therapy (HSC-GT) improved enzyme activity, cognitive function, and repopulation of CNS microglia and PNS macrophages (76). Clinical trials involving pre-symptomatic late-infantile patients and early-symptomatic early-juvenile patients confirmed the sustained benefits of HSC-GT therapy without significant safety concerns, while improving motor function and survival rates compared to untreated individuals (66, 77). However, patients in advanced stages of MLD did not benefit from the therapy, indicating that the level of cell engraftment and the timing of treatment in relation to disease onset are crucial factors for a positive outcome (66).

OTL-200 (atidarsagene autotemcel) was approved as the first HSC-GT for MLD in 2020 under the commercial name Libmeldy (Orchard therapeutics). Recently, Libmeldy has also been accepted as a therapeutic option for MLD patients in Norway (78). Treatment is only an option for pre-symptomatic patients or early-symptomatic patients if treated before the onset of rapid disease-progression (66, 77). Early diagnosis of MLD is therefore crucial to ensure optimal effect of treatment. MLD has now been confirmed to be on its way into the newborn screening program in Norway, providing hope for future affected families (78).

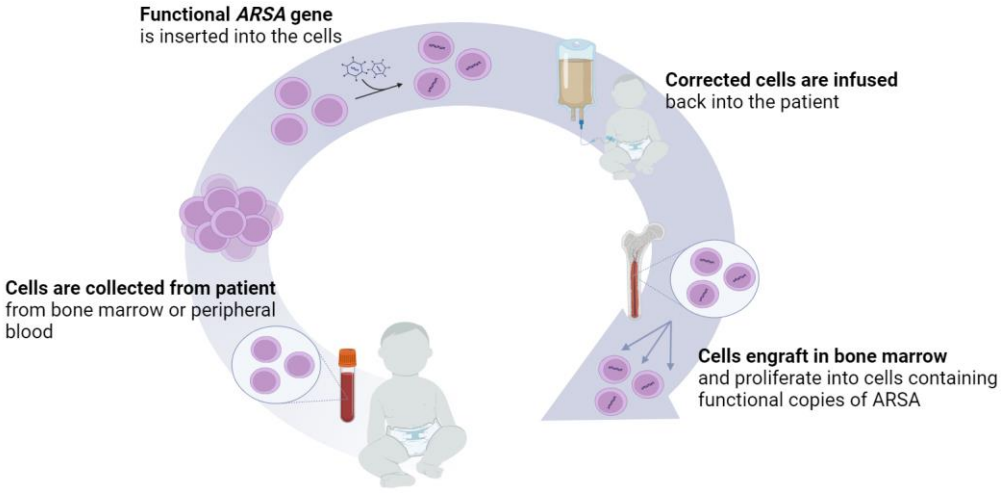

Figure 1.6. Principle of hematopoietic stem cell gene therapy (HSC-GT) for treating MLD. HSC-GT begins with the extraction of hematopoietic stem cells from the patient. Cells are genetically modified *in vitro* to introduce functional copies of the *ARSA* gene using viral vectors. Modified cells with functional copies of *ARSA* are infused back into the patient and engraft in the bone marrow. Gene-corrected cells begin to produce functional ARSA enzyme, restoring ARSA levels to prevent MLD disease progression. Figure created in Biorender.com.

2. Objectives

MLD is a severe disease that has detrimental effects on both patients and their families (21, 31, 33). While recent advancements in medical science have resulted in emerging treatment options, there is still an absence of effective therapy for symptomatic patients (66, 77). Although the relation between MLD and subsequent demyelination has been established, the pathomechanisms behind this process remain largely unknown (21). This highlights the importance of further research on MLD, particularly the intricate pathomechanisms driving the demyelination that characterizes the disease. Understanding MLD requires effective models that recapitulate the disease progression observed in humans. Human induced pluripotent stem cells (hiPSCs) are particularly promising, as they allow for the detailed study of the disease's development specific to patients with MLD, and comparisons with healthy controls.

The aim of this thesis is to provide basis for further investigations of the underlying MLD pathomechanisms, by establishing MLD-specific hiPSCs. The two primary research objectives are to: (i) generate hiPSCs as a study model for MLD and (ii) compare pluripotency, maturation and genome stability markers and properties between hiPSCs derived from MLD patients and those from healthy individuals.

3. Materials and Methods

3.1. Cells and cell culture

3.1.1. Cell lines

All cells were grown at 37 °C, 5% CO_2. PBMCs used for reprogramming to hiPSCs were obtained from a donor family (MLD family 3), which included a patient with MLD (♂ARSA$^{mut/mut}$), and healthy carrier parents (♀ARSA$^{wt/mut}$ and ♂ARSA$^{wt/mut}$). The affected MLD patient contains the mutations c.465+1G>A and c.1283C>T, inherited from the mother and father respectively (Figure 3.1).

hiPSC samples from two additional MLD-affected families (MLD family 1 and 2) were used in the assessment of stemness markers expression between families affected by MLD, and have previously been reprogrammed from PBMCs in our lab by Rabina Dumaru (unpublished findings). Affected MLD patients from the two families had the same two mutations, consisting of c.370G>C and c.465+1G>A.

hiPSCs from a fibroblast-derived cell line (GM00243) were utilized during neural differentiation to O4+ oligodendrocytes (subsection 3.7). The GM00243 cell line originates from a male child affected by MLD, containing the homozygous mutation c.465+1G>A (79). Fibroblasts were obtained from Coriell Institute and have previously been reprogrammed and characterized in our lab. The media in which iPSCs were grown are indicated in each of the methods below. The PBMCs were isolated and iPSCs generated as part of the REK-456339.

A control HEK293T cell line (ATCC, USA) was used during analysis of DNA damage levels in hiPSCs (subsection 3.6). HEK293T cells were cultured in DMEM High Glucose Medium (Sigma-Aldrich, D6429) supplemented with 10% Fetal Bovine Serum (FBS) (Sigma, F7524) and 1X Penicillin-Streptomycin (P/S) (Gibco, 15140122).

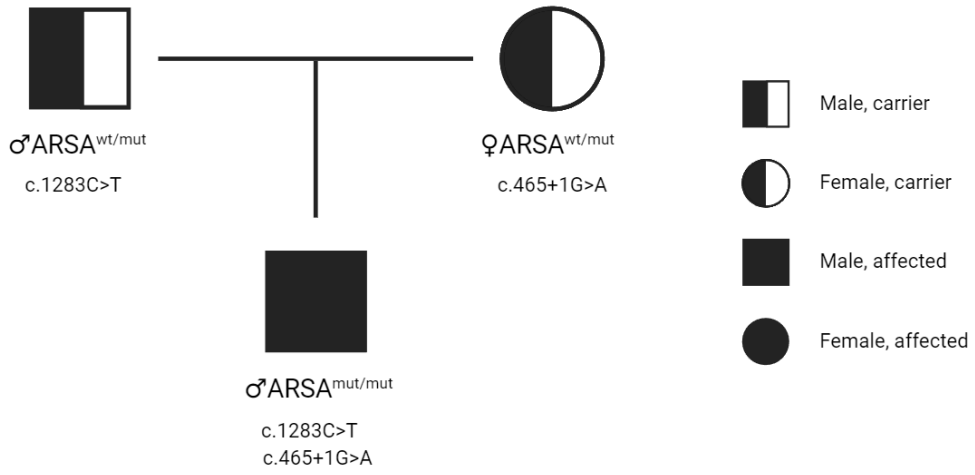

Figure 3.1. Pedigree of *ARSA* mutations in a family affected by MLD.
Affected child of MLD (♂ARSA$^{mut/mut}$) contains the mutations c.465+1G>A and c.1283C>T inherited from carrier mother and father respectively (♀ARSA$^{wt/mut}$ and ♂ARSA$^{wt/mut}$)

3.1.2. Reprogramming PBMCs using Sendai Virus

PBMCs were isolated from blood samples retrieved from MLD family donors and stored in liquid nitrogen. Upon use, PBMCs were thawed, resuspended in Expansion medium (Table A.1) and seeded in a 12-well suspension plate at a concentration of 1 x 10^6 cells/well. Cells were incubated for 9 days, performing medium changes every 3 days, until 80% cell confluency. Figure 3.2 depicts a schematic overview of the reprogramming process.

Cells were transfected with Sendai Virus containing reprogramming factors according to CytoTune™-iPS 2.0 Sendai Reprogramming Kit (Invitrogen, A16517). Briefly, 3 x 10^5 cells per donor-sample were transfected with virus containing appropriate multiplicity of infection (MOI) (KOS:hc-Myc:hKlf4=5:3:3) in 1 ml expansion media containing 4 µg/ml polybrene (Sigma-Aldrich, H9268). Transfected cells were transferred to 2 wells per donor in a 12-well suspension plate, and were incubated at 37 °C, 5% CO_2 for 24 h. Media was changed to expansion media without polybrene and incubated for 2 more days.

3 days post-infection, cells from each well were transferred to a 10 cm culture dish containing irradiated CF1 mouse-embryonic fibroblasts (MEFs) (1.7 x 10^6 cells/dish, Gibco, A34181), and cultured for 2 more days in expansion media. Cells were then maintained in hiPSC medium (see Table A.2) for the next 30 days. Around 8 days post transfer to MEFs, iPSC colonies started to appear. Undifferentiated colonies were picked

and transferred to geltrex (Gibco, A1413202)-coated 12-well plate and maintained in E8 medium as described for hiPSCs (subsection 3.1.3). Each transferred colony from the 10 cm dish was characterized as distinct hiPSC clones for each donor. In the next passage, cells were split 1:1 to a well of a geltrex-coated 6-well plate. The following passage was done in a 1:3 ratio to three wells of a 6-well plate. Cell pellets were collected at passage 6 for karyotyping and stemness marker analysis. Cells were propagated until passage 8 and subsequently frozen as described in subsection 3.1.4.

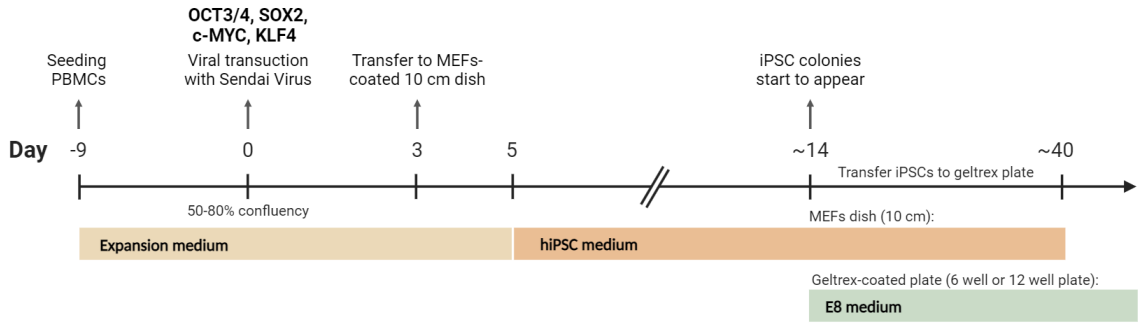

Figure 3.2. Schematic overview of hiPSC generation from PBMCs using Sendai Virus. PBMCs were expanded for 9 days and were then transduced with Sendai Virus containing reprogramming factors (OCT3/4, SOX2, c-MYC, KLF4). On day 3, cells were seeded on MEFs. Two days later cells were kept in hiPSC medium and cultured until day 40. Undifferentiated iPSC colonies started to appear on day 14 and were transferred to geltrex-coated plates and cultured in E8 medium. Figure created in Biorender.com.

3.1.3. hiPSC cell culture

hiPSCs were primarily cultured in Essential 8 (E8) Medium (Gibco, A1517001) supplemented with 1 % P/S on 6-well plates (Corning, Costar) coated with 1% geltrex. Daily medium change was performed until cells reached 70-90% confluency. Passaging of cells was done by washing with DPBS (Gibco, 14190-144) and treating the cells with EDTA (0.5 mM in DPBS) (Invitrogen, 15575020) at room temperature (RT) for 2-3 min. Cells were sprayed with E8 medium containing 10 µM Rock inhibitor Y-27632 (ROCKi) (Millipore, 688000). Detached cells were transferred to splitting medium at 1:3 ratio. 1.5 mL of cell suspension was seeded per well of a geltrex-coated 6-well plate and incubated for 24 h. Cells were washed with DPBS (Gibco, 14190-144) and medium was changed to E8 without ROCKi.

3.1.4. Cryopreserving and thawing hiPSCs

Cryopreservation of hiPSCs was performed by washing with DPBS and treatment with EDTA as in passaging. Cells were detached by spraying 1 ml/well freezing media (90% E8 medium + 10% DMSO (Sigma-Aldrich, D2650)). Cells were transferred to cryotube and stored with step-wise cooling at -80 °C over night (O/N). Cells were placed in liquid nitrogen for long term storage.

For thawing hiPSCs, cryovial containing hiPSCs was placed in water bath (37 °C) until a small piece of ice remained. Cell suspension was transferred to an empty 15 ml falcon, and E8 medium (6 ml) containing 10 µM ROCKi was added slowly. Cells were centrifuged at 200 x *g* for 5 min. Pellet was resuspended in E8 medium (2 ml) with 10 µM ROCKi, and cells were seeded on geltrex-coated 6-well plate.

3.2. Karyotyping

hiPSCs were assessed for 8 common chromosomal abnormalities using hPSC Genetic Analysis Kit (StemCell technologies, 07550) according to the manufacturer's protocol. DNA was initially isolated from cell pellets by using DNeasy Blood and Tissue Kit (Qiagen, 69506) and 50 µl TAE buffer (10 mM Tris-Cl, 0.5 mM EDTA; pH 9.0) was added to elute DNA. DNA concentration was determined using NanoDrop ND-1000. qPCR was performed with StepOnePlus Real-Time PCR system (Applied Biosystems) and primers provided in the hPSC Genetic Analysis Kit, using TaqMan program, standard cycling time = 3 min.

3.3. Embryoid body (EB) formation

hiPSCs were cultured until 80-90% confluency and treated with accutase (StemCell Technologies, 07920) for 2-3 min until cells detached. Cells were transferred to DMEM/F12 (Gibco, 11330032) and centrifuged for 5 min at 200 x *g*. Cell pellet was resuspended in E8 medium with 10 µM ROCKi and 6 x 10^5 cells were seeded per well in an ultra-low attachment plate (Corning, 3471). Cells were incubated (37 °C, 5% CO2) on orbital shaker O/N allowing EBs to form. Remaining cell suspension was pelleted by centrifugation at 200 x *g* for 5 min at 4 °C. Cell pellet was washed with DPBS and centrifugation was repeated before storing cells as Day 0 pellet at -80 °C. Medium change to EB medium (Table A.3) was performed the following day (Day 1) and on Day 3. On day 4, EBs were pelleted and stored at -80 °C as Day 4 pellet.

3.4. RNA Isolation and RT-qPCR

RNA was isolated from cell pellets using the RNeasy mini kit (Qiagen, 74106) and RNase-free DNase Set (Qiagen, 79254) according to the manufacturer's protocol, using 40 µl of RNase-free water for RNA elution. RNA concentration was measured with NanoDrop ND-1000 and stored at -20°C until cDNA synthesis. RNA was diluted to 10 ng/µl in 20 µl RNase-free water, and cDNA was synthesized using High-Capacity cDNA Reverse Transcription Kit (Applied Biosystems, 4368814) according to manufacturer's protocol without RNase inhibitor. Synthesized cDNA was diluted 1:10 and stored at -20 °C until use. Master Mixes for markers were prepared with POWER SYBR® Green Master Mix 2X (Applied Biosystems, 4367659), forward and reverse primer (10 µM) for each respective target (Table A.4). cDNA (1:10 dilution, 2 µl) and Master Mix (8 µl) were distributed per well of a 96-well qPCR plate (Sarstedt), and qPCR was performed in StepOnePlus Real-Time PCR system.

3.5. Immunofluorescence analysis

For immunofluorescence analysis, hiPSCs were seeded onto coverslips placed in geltrex-coated 6-well plate and cultured as described in subsection 3.1.3. When cells reached 70% confluency, they were fixed with 4% paraformaldehyde (PFA) (15 min, RT) and washed with DPBS (5 min, 3 times) on shaker (16 rpm). Permeabilization and blocking was performed by incubating cells in Blocking buffer (prepared in PBS: 5% BSA (Sigma-Aldrich, A9418), 5% goat serum (Invitrogen, 10000C), and 0.1% Triton X-100 (Sigma-Aldrich, T8787)) on shaker (16 rpm, 1 h, RT).

Primary antibody solutions were prepared by diluting antibodies in their respective dilution, as listed in Table A.5, in PBS containing 0,1% Triton X-100, 0,5% BSA, 0,5% goat serum. hiPSCs on coverslips were incubated in 30 µl primary antibody solution at 4 °C O/N. Cells were washed on shaker in PBS-T (3 x 5 min, RT, 16 rpm). Secondary antibody solutions were prepared by diluting both Alexa Fluor 594 goat anti-rabbit (Thermo Fisher, A11037) and Alexa Fluor 488 donkey anti-mouse (Thermo Fisher, A21202) 1:500 in PBS-T (0,1%). Coverslips were kept in dark following this step and incubated in 30 µl secondary antibody solution for 1 h at RT. Cells were subsequently washed on shaker in PBS-T (3 x 5 min, RT, 16 rpm). Cells were stained and incubated with DAPI solution (1 µg/ml in PBS, Thermo Scientific, 62248)) for 15 min on shaker (16 rpm), and were washed with PBS on shaker (3 x 5 min, RT, 16 rpm). 15 µl ProLong Gold Antifade Mountant with DNA Stains DAPI (Invitrogen, P36931) was added to glass slide to mount coverslips. Slides were placed in a dark chamber at RT O/N to dry, and stored at 4 °C for long time storage. Imaging was performed in EVOS FL Auto Cell Imaging System. Microscope settings are described in Table A.6.

3.6. Comet assay

For positive control, 8 x 10^5 cells/well (HEK293T) were seeded in a 6-well plate, and were detached with trypsin/EDTA (Sigma-Aldrich, T3924) the following day at 40-50% confluency. Cells were centrifuged at 200 x *g* for 2 min at 4 °C and resuspended in 100 µM H_2O_2 (1 ml per well). Cells were incubated for 30 min on ice, protected from light. Cells were centrifuged at 200 x *g* for 2 min at 4 °C, resuspended in cold PBS and aliquoted

in 250 000 cells/tube. Cells were snap-frozen in liquid nitrogen and stored at -80 °C until use.

hiPSCs were detached with accutase, transferred to DMEM/F12 and centrifuged at 200 x *g* for 5 min at RT. Cell pellet was resuspended in cold PBS, centrifuged at 200 x *g* for 2 min at 4 °C and a 60 000 cells/ml dilution was prepared in cold PBS. Cells were prepared in 1% Low Melting Point Agarose (Lonza, 50100) in a 1:10 ratio, and cell suspension (40 µl) was immediately distributed on Comet Slide (R&D systems, 4250-200-03) with two replicates per sample. Slides were dried in the dark at 4 °C for 15 min, and then submerged in Lysis Buffer (2.5 M NaCl, 100 mM EDTA, 1% TRIS base, 1% lauroylsarcosine sodium salt, 1% Triton X-100, 10% DMSO) on ice for 1 h. Slides were washed two times for 10 min in fresh Alkaline Unwinding Solution (pH >13, 200 mM NaOH, 1 mM EDTA), and then placed in a Comet Assay Tank containing Alkali Unwinding Solution where electrophoresis was run at 25 V, 300 mA for 20 min. Slides were washed in dH2O two times for 10 min, and in ethanol (70%) for 5 min while protected from light. Slides were then dried at 37 °C for 30 min. SYBR® Green (Invitrogen, 57563, 1:10 000 dilution in TE buffer (10 mM TRIS HCl, 1 mM EDTA) was added to each well, and incubated at 4 °C for 15 min in the dark. Slides were washed with dH2O two times for 10 min and were let to dry O/N at RT in a dark chamber with silica gel beads. Imaging was performed the following day in EVOS FL Auto Fluorescence Microscope, capturing 30-40 images per replicate. Analysis was performed using Comet Assay IV Software (Instem, Perceptive Instruments). Microscope settings are described in Table A.6.

3.7. Neural differentiation of hiPSCs to O4+ oligodendrocytes

hiPSC were passaged as described in subsection 3.1.3, and medium was changed the next day to E8 + mTESR1 medium (StemCell Technologies, 85850) in a 1:1 ratio, increasing the concentration of mTESR1 to 100% the following day. Medium changes were performed daily until 70-90% confluency. Cells were detached with accutase and seeded in a geltrex-coated 6-well-plate with a 2.5 x 10^5 cells/well distribution containing mTESR1 medium and 1X RevitaCell (Gibco, A2644501). Cells were incubated for 48 h, allowing the formation of colonies with ~100 µm diameter. Medium was changed to N2B27 medium (Table A.7) supplemented with 0.1 µM RA (Sigma-Aldrich, R2625), 10

µM SB431542 (StemCell Technologies, 72234) and 1 µM LDN193189 (Miltenyi Biotech, 130-106-540), performing daily medium changes for 5 days. 10 µM SAG supplement (Millipore, 566660) was then added to the medium in addition to other supplements, and cells were cultured for 2 more days.

On day 7, cells were detached with accutase and 1.25 x 10^6 cells per well were seeded on a Poly-L-ornithine (50 µg/ml, Sigma-Aldrich, P4957) and Laminin (10 µg/ml, R&D Systems, 3446-005-01)-coated 6-well plate in N2B27 medium (supplemented with 0.1 µM RA, 10 µM SAG, 1X RevitaCell). Viral transduction was performed the following day to induce sex determining region Y-box 10 (SOX10) overexpression by using the lentiviral vectors FUW-TetON-SOX10 (Addgene, 115242) and FUW-M2rtTA (Addgene, 20342) in a 1:1 ratio. On the next day, medium was changed to Oligodendrocyte differentiation medium (see Table A.8) containing 1 µg/ml doxycycline (Sigma-Aldrich, D9891), and cultured for 9 days performing medium changes every other day. See Figure 3.3 for schematic overview of differentiation protocol.

Ten days post viral transduction, cells were resuspended in MACS buffer (1x PBS with 2mM EDTA and 0.5% BSA), and O4+ cells were isolated using Anti-O4 microbeads (Miltenyi Biotec, 130-094-543) running through an LS column (Miltenyi Biotech, 130-042-401). Eluted O4+ cells were resuspended in freezing medium (Oligodendrocyte differentiation medium containing 10% DMSO) and frozen as described in subsection 3.1.4.

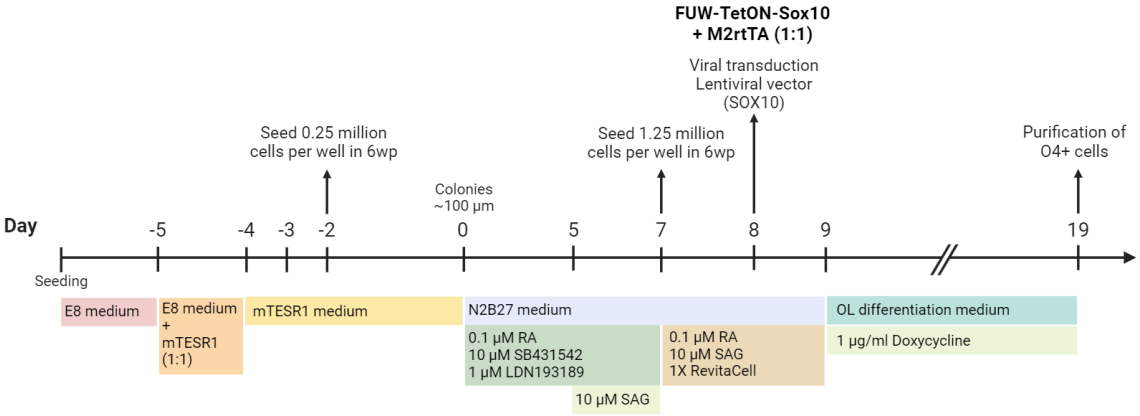

Figure 3.3. Schematic overview of neural differentiation of hiPSCs to O4+ oligodendrocytes. hiPSC were cultured in E8 and mTESR1 medium until colonies were 100 µM in diameter. Neural induction to OLIG2+ progenitor cells was induced by culturing cells in N2B27 medium with appropriate supplements until day 8. Cells were transduced with a lentiviral vector containing viral vectors FUW-TetON-Sox10 and FUW-M2rtTA to induce SOX10 overexpression. Oligodendrocyte (OL) differentiation medium was used as a culture medium to drive the cells towards the O4+ oligodendrocyte lineage. The figure was created in BioRender.

3.8. Statistical analysis

Statistical differences were determined using one-way ANOVA with Tukey's multiple comparisons test in GraphPad Prism v.10 (GraphPad Software, Inc.). Error bars represent mean ± SEM. Differences were considered significant at *$p < 0.05$, **$p \leq 0.01$, ***$p \leq 0.001$, and ****$p \leq 0.0001$. Non-significant values are noted as ns ($p \geq 0.05$).

4. Results

4.1. Generation of hiPSCs from individuals of a family affected by MLD

iPSCs offer a valuable model for studying the cellular mechanisms underlying genetic disorders, including MLD. In this study, hiPSCs were successfully generated by reprograming PBMCs isolated from three individuals in a family affected by MLD: an affected child (♂ARSA$^{mut/mut}$), and carrier parents (♀ARSA$^{wt/mut}$ and ♂ARSA$^{wt/mut}$) (Figure 4.1). This resulted in the generation of multiple clones per individual, which were subsequently evaluated based on pluripotent morphology and stable growth characteristics in culture. The five hiPSC clones from ♂ARSA$^{mut/mut}$ (cl. 8.1, 8.2, 8.3, 8.8 and 8.9), ♀ARSA$^{wt/mut}$ (cl. 9.1, 9.2, 9.6, 9.7 and 9.8) and ♂ARSA$^{wt/mut}$ (cl. 10.1, 10.3, 10.6, 10.9 and 10.10) were selected based on their growth rate and morphology for further analysis.

Upon thawing of the clones, notable differences in the culturing efficiency and cellular behavior were observed among the hiPSCs derived from the different donors. Specifically, ♂ARSA$^{wt/mut}$ exhibited challenges related to reduced cell attachment, increased cell death and a higher tendency for spontaneous differentiation, resulting in a greater presence of non-iPSCs.

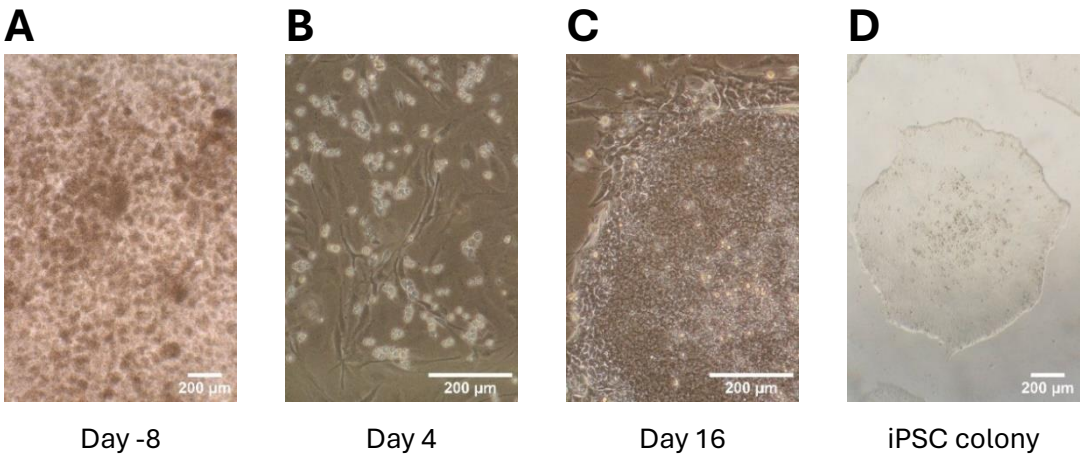

Figure 4.1. Reprogramming of PBMCs to hiPSCs during different stages of differentiation. Representative images from different stages of reprogramming and isolated iPSC colony. **A.** PBMCs in 12-well suspension plate the day after seeding. **B.** PBMCs seeded on MEFs-coated 10 cm dish. Day 4 post-transduction. **C.** Emerging undifferentiated iPSC colony on MEFs-coated dish 16 days post-transduction. **D.** Representative image of iPSC colony after transfer to geltrex-coated plate. Scale bars = 200 µm.

4.2. Analysis of chromosomal copy numbers in hiPSC clones

The process of reprogramming somatic cells to iPSCs can often lead to changes in genome integrity, resulting in the accumulation of chromosomal aberrations, such as copy number variants (CNVs) (80). hiPSC clones derived from the three MLD-affected individuals, ♂ARSA$^{mut/mut}$ (cl. 8.1, 8.2, 8.3, 8.8 and 8.9), ♀ARSA$^{wt/mut}$ (cl. 9.1, 9.2, 9.6, 9.7 and 9.8) and ♂ARSA$^{wt/mut}$ (cl. 10.1, 10.3, 10.6, 10.9 and 10.10), were therefore assessed by RT-qPCR analysis for variations in copy number within the eight most common mutated regions in human pluripotent stem cells.

The expected copy number for each autosomal chromosome is 2, and deviations from this indicates potential chromosomal abnormalities, such as regional deletions or duplications. An exception of this regards the X chromosome, expected to be equal to 1 in males (♂ARSA$^{mut/mut}$ and ♂ARSA$^{wt/mut}$). Karyotyping analysis revealed variabilities in chromosomal copy numbers across the hiPSC clones from each individual (Figure 4.2). Clones were evaluated and ranked according to their genomic stability, and the three clones with the least deviation from the expected diploid copy number were chosen for further analysis promising. Based on this, clone 8.2, 8.8, and 8.9 from ♂ARSA$^{mut/mut}$, clone 9.7, 9.8, and 9.2 from ♀ARSA$^{wt/mut}$ and clone 10.1, 10.3, and 10.9 from the ♂ARSA$^{wt/mut}$ were determined to have the highest degree of genome integrity.

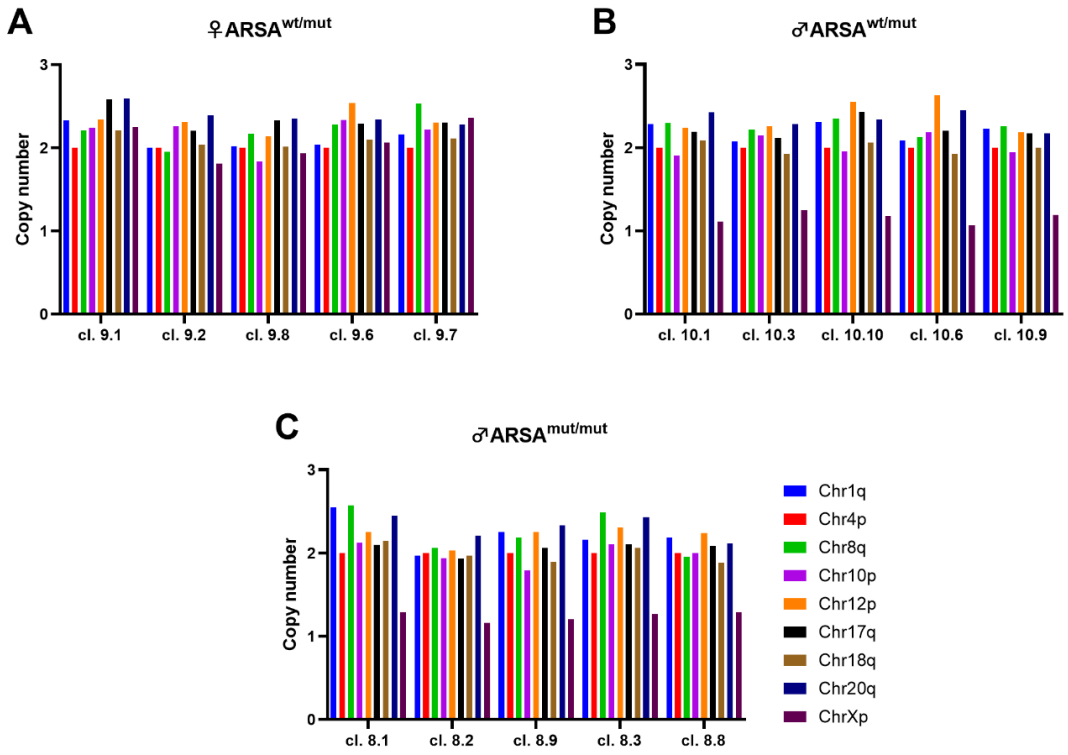

Figure 4.2. Copy number variations (CNVs) in hiPSC clones based on karyotyping.
Copy numbers of eight chromosomal locations in **A.** ♀ARSA$^{wt/mut}$ (cl. 9.1, 9.2, 9.6, 9.7 and 9.8) **B.** ♂ARSA$^{wt/mut}$ (cl. 10.1, 10.3, 10.6, 10.9 and 10.10) and **C.** ♂ARSA$^{mut/mut}$ (cl. 8.1, 8.2, 8.3, 8.8 and 8.9). Values normalized to the internal control, Chr4p.

4.3. Expression of pluripotency markers in hiPSCs

4.3.1. Immunofluorescence analysis validates expression of pluripotency markers OCT4 and SSEA4

IF analysis was performed to assess the levels of pluripotency markers OCT4 and SSEA4 in hiPSCs, to ensure their undifferentiated state and validate their quality for further experiments and characterization. Clones from each individual, ♂ARSA$^{mut/mut}$ (cl. 8.2, cl. 8.8 and cl. 8.9), ♀ARSA$^{wt/mut}$ (cl. 9.7 and 9.8) and ♂ARSA$^{wt/mut}$ (cl. 10.9 and 10.1), were analyzed (Figure 4.3 A).

DAPI was used as control to localize the nuclei of the cells. OCT4 was found to be expressed within the nucleus for each sample (Figure 4.3 B). SSEA4 exhibited expression across the entirety of the iPSC colonies, consistent with its membrane-associated localization (Figure 4.3 C).

Quantitative analysis of OCT4 and SSEA4 signal was performed for each sample, utilizing the mean intensity derived from the IF images. No significant differences in signal intensities were detected between the individuals. The consistent expression levels of OCT4 and SSEA4, combined with the absence of significant differences between individuals, suggest a stable and uniform pluripotent phenotype across the hiPSCs from the MLD-affected individuals.

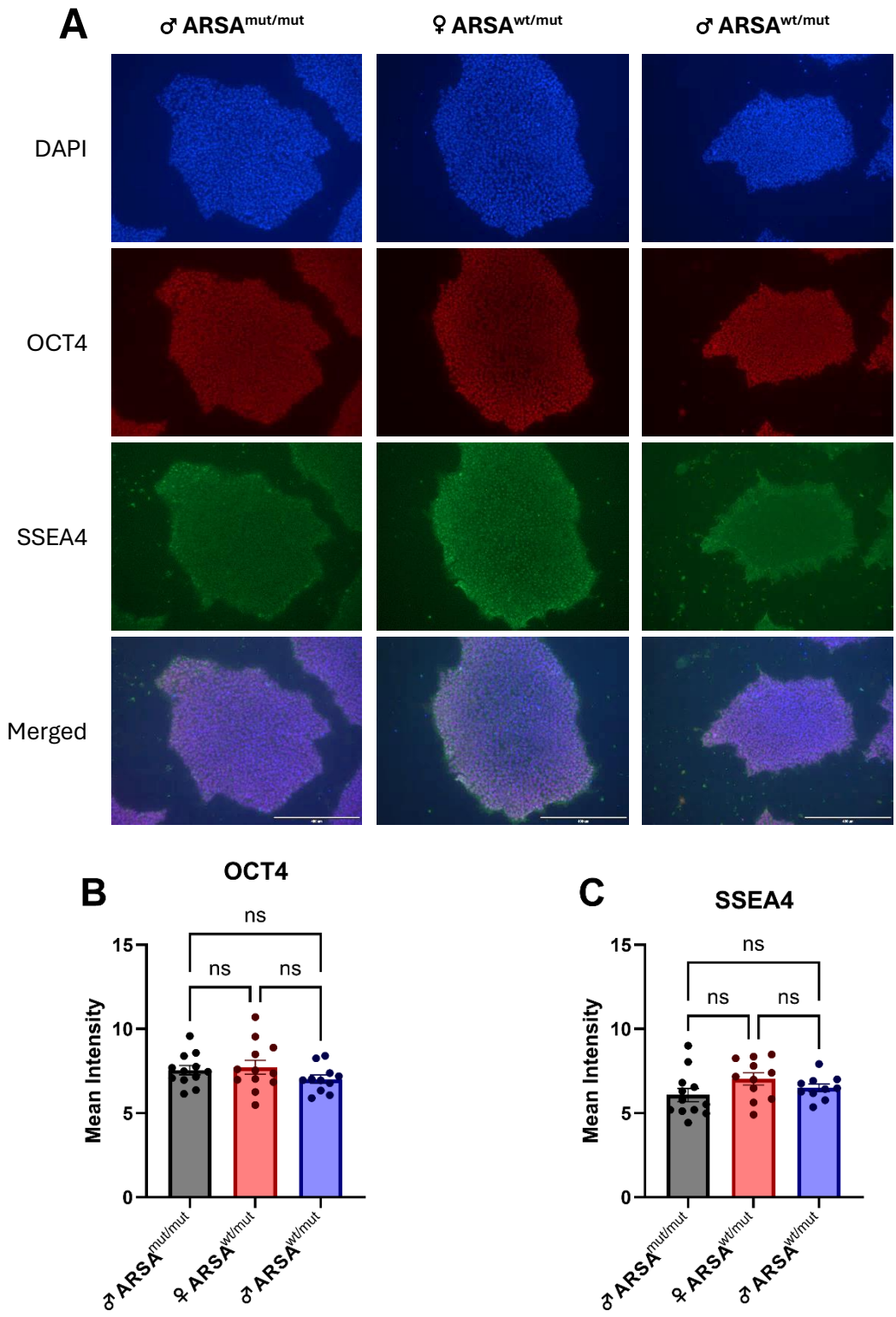

Figure 4.3. Immunofluorescence analysis of pluripotency the markers OCT4 and SSEA4 in hiPSCs.

A. Representative IF images of DAPI (blue), OCT4 (red), SSEA4 (green) and markers merged in hiPSCs from ♂ARSA$^{mut/mut}$, ♀ARSA$^{wt/mut}$ and ♂ARSA$^{wt/mut}$. Scale bars = 400 µm **B.-C.** Mean intensity of OCT4 (B) and SSEA4 (C) staining in hiPSCs based on IF analysis. Data from three independent experiments consisting of four technical replicates per individual, using ♂ARSA$^{mut/mut}$ (cl. 8.2, cl. 8.8 and cl. 8.9), ♀ARSA$^{wt/mut}$ (cl. 9.7 and 9.8) and ♂ARSA$^{wt/mut}$ (cl. 10.9 and 10.1). Error bars represent mean ± SEM. One-way ANOVA was used to determine statistical significance, followed by Tukey's multiple comparisons test, ns=$p \geq 0.05$.

4.3.2. Gene expression analysis of OCT4, SOX2 and NANOG levels in individuals from three MLD-affected families

To further evaluate the expression of pluripotency markers in MLD-derived hiPSCs, RT-qPCR analysis targeting OCT4, SOX2, and NANOG was performed (Figure 4.4 A, B, and C, respectively). In addition to hiPSCs derived from MLD family 3 (MLD8, MLD9 and MLD10), expression of pluripotency markers was assessed for hiPSCs derived from two additional MLD-affected families, MLD family 1 (MLD1, MLD2, MLD3) and MLD family 2 (MLD5, MLD6, MLD7). Each family comprises an affected child diagnosed with MLD, and both parents are identified as carriers (subsection 3.1.1). Multiple MLD-affected individuals were used in the analysis to explore whether variations in the expression of pluripotency markers could correlate with the genetic differences between affected individuals and carriers within and across families. Three experiments were performed for each individual from the three families, consisting of three clones from each individual.

For OCT4, the expression levels were generally consistent across the different samples. Notably, one of the affected patients (MLD5) exhibited a significant reduction in OCT4 expression compared to individuals from MLD family 1. Individuals from MLD family 1 displayed a modest trend toward higher OCT4 expression in comparison to the other families. However, this trend is not considered statistically significant. The overall expression profile of OCT4 indicates a comparable expression of this pluripotency marker among the analyzed individuals.

In assessment of SOX2, a slight variation in expression levels was observed between the two individuals demonstrating the maximal and minimal gene expression (MLD1 and MLD7). Despite these minor differences, the collective expression of SOX2 remained primarily uniform, suggesting that no individual or family exhibits SOX2 levels that significantly deviate from the other samples.

Regarding NANOG, the expression was comparable across all samples, showing no significant differences between the samples. These findings, along with the mainly uniform expression of OCT4 and SOX2, suggest a stability of pluripotency marker expression between the individuals and among the different families included in this experiment.

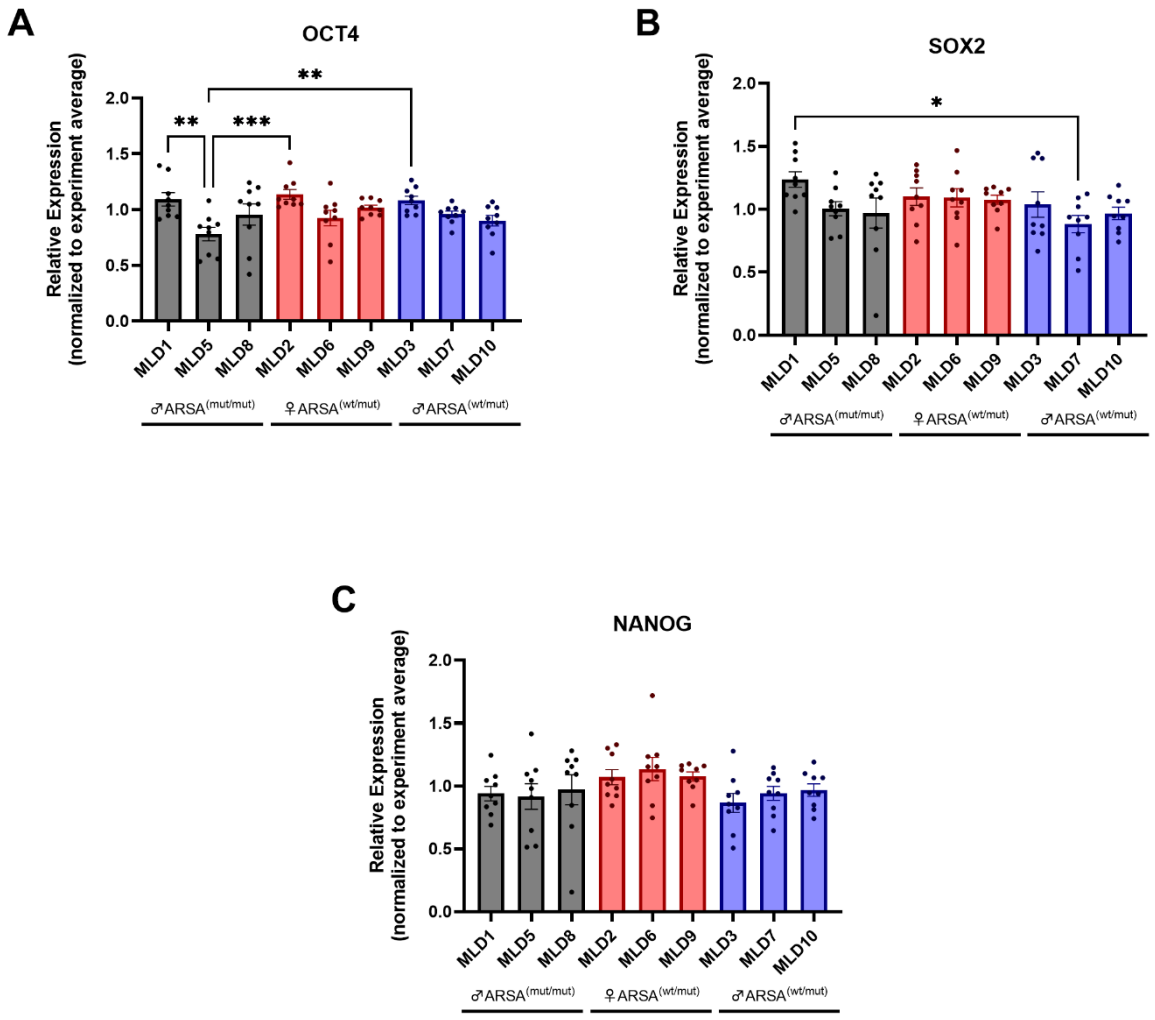

Figure 4.4 Gene expression analysis of pluripotency markers OCT4, SOX2 and NANOG in hiPSCs.

Relative mRNA levels of **A**. OCT4, **B**. SOX2, **C**. NANOG in hiPSCs derived from individuals of three MLD-affected families consisting of ♂ARSA$^{mut/mut}$ (MLD1, MLD5 and MLD8), ♀ARSA$^{wt/mut}$ (MLD2, MLD6 and MLD9) and ♂ARSA$^{wt/mut}$ (MLD3, MLD7 and MLD10) including 3 clones per individual. Error bars represent mean ± SEM. Statistical significance between groups is noted by *$p < 0.05$, **$p \leq 0.01$, ***$p \leq 0.001$.

4.4. EB formation and expression of germ layer markers

EB formation was performed for hiPSCs from ♂ARSA$^{mut/mut}$ (cl. 8.2, cl. 8.8 and cl. 8.9), ♀ARSA$^{wt/mut}$ (cl. 9.7 and 9.8) and ♂ARSA$^{wt/mut}$ (cl. 10.9 and 10.1) to assess pluripotency state and differentiation potential (Figure 4.5. A). Several EB formations were attempted per clone, with varying successful outcome and EB quality. RT-qPCR was utilized to measure the expression of germ layer markers in EBs compared to cells as hiPSCs.

Expression of the pluripotency marker OCT4 was assessed to ensure that cells were transitioning towards a differentiated state, where pluripotency markers are expected to decrease. Expression of OCT4 was observed to decrease in hiPSCs from each individual (Figure 4.5 B), confirming the initiation of differentiation away from a pluripotent stage.

Analysis of the endodermal markers GATA4 and SOX17 exhibited a slight increase in expression levels as the hiPSCs transition to EBs, indicative of the differentiation process towards endodermal lineages (Figure 4.5. C and D respectively). However, the increase in ♂ARSA$^{wt/mut}$ was considerably less pronounced than the others, suggesting that this genotype may have a diminished endodermal differentiation potential.

Expression of the mesodermal markers FOXC1 and BMP4 were found to be upregulated upon differentiation to EBs, although in varying degrees across the genotypes (Figure 4.5. E and F respectively). Consistent with the expression of the endodermal markers, ♂ARSA$^{wt/mut}$ exhibited a less marked increase in FOXC1 expression upon differentiation compared to other genotypes. BMP4 expression was comparable between ♂ARSA$^{mut/mut}$ and ♂ARSA$^{wt/mut}$. A comparable increase for the ectodermal marker NESTIN was observed in each individual (Figure 4.5. G). However, the upregulation was moderate, accompanied by variations among the clones.

PAX6 was initially included to assess ectodermal differentiation (not shown). However, PAX6 expression was predominantly below the detection limit in both hiPSCs and EBs, with only sporadic values slightly above the threshold. Due to low and inconsistent expression levels, PAX6 was therefore not included.

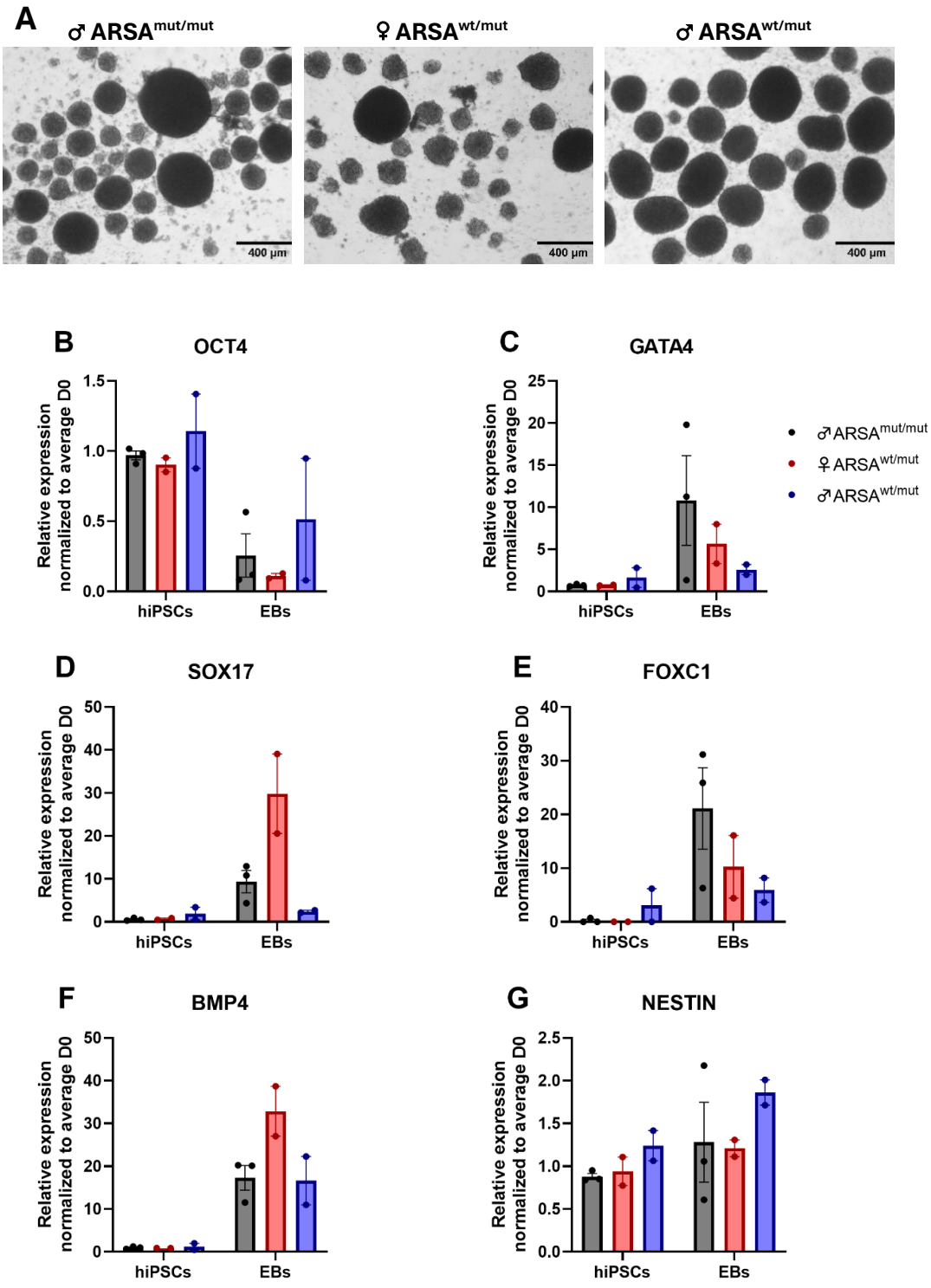

Figure 4.5. Gene expression analysis of germ layer markers in hiPSCs and embryoid bodies. **A.** Representative images of embryoid bodies (EBs) from each individual at day 3. Scale bars = 400 µm. **B.-G.** Relative mRNA levels in of pluripotency marker OCT4 (B) and germ layer markers GAT4 (C), SOX17 (D), FOXC1 (E), BMP4 (F) and NESTIN (G) in hiPSCs and EBs from ♂ARSA$^{mut/mut}$ (cl. 8.2, cl. 8.8 and cl. 8.9), ♀ARSA$^{wt/mut}$ (cl. 9.7 and 9.8) and ♂ARSA$^{wt/mut}$ (cl. 10.9 and 10.1). Expression of each marker is normalized to average value of hiPSCs. Data from one experiment including 2-3 clones for each individual. Error bars represent mean ± SEM.

4.5. Assessment of proliferation rate between hiPSCs

Proliferation rate is a fundamental parameter that reflects the health and viability of hiPSCs, and should be comparable across different clones and individuals to be used as reliable samples in further studies. Expression of the proliferation marker Ki67 was therefore assessed by IF analysis in hiPSC clones from the three MLD-affected individuals (Figure 4.6 A).

The analysis of Ki67+ cells revealed no significant differences in the proliferation rates among the hiPSCs derived from ♂ARSA$^{mut/mut}$ ♀ARSA$^{wt/mut}$ and ♂ARSA$^{wt/mut}$. (Figure 4.6 B). These findings further reinforce that the hiPSCs used in this study are stable and maintain a consistent rate of proliferation. This stability is advantageous for ensuring that any future experiments are not influenced by variations in cell proliferation rates, which allows for a more accurate assessment of disease-specific effects.

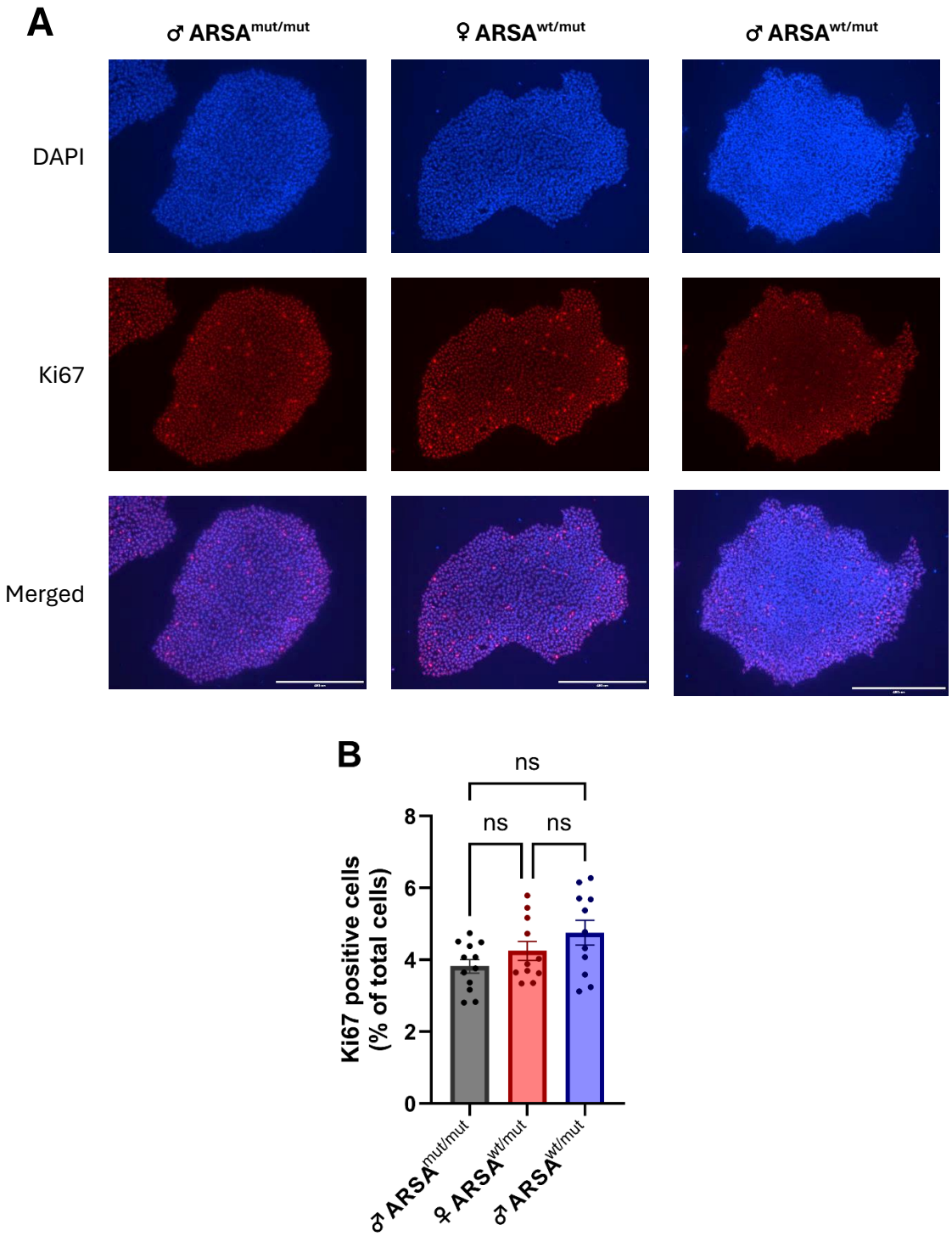

Figure 4.6 Immunofluorescence analysis of proliferation marker Ki67 in hiPSCs.
A. Representative IF analysis images of DAPI (blue), Ki67 (red) and markers merged in hiPSCs Ki67 (red) and in hiPSCs from ♂ARSA$^{mut/mut}$, ♀ARSA$^{wt/mut}$ and ♂ARSA$^{wt/mut}$. Scale bars = 400 µm **B.** Percentage of Ki67+ cells in hiPSCs based on IF analysis from each individual. Each datapoint represents the average percentage of Ki67+ cells from one coverslip. Data from three biologically independent experiments consisting of four technical replicates per individual, using at least two clones. The clones used were ♂ARSA$^{mut/mut}$ (cl. 8.2, cl. 8.8 and cl. 8.9), ♀ARSA$^{wt/mut}$ (cl. 9.7 and 9.8) and ♂ARSA$^{wt/mut}$ (cl. 10.9 and 10.1). Error bars represent mean ± SEM. One-way ANOVA was used to determine statistical significance, followed by Tukey's multiple comparisons test, ns = $p \geq 0.05$.

4.6. Variable levels of DNA damage across hiPSCs from MLD-affected individuals

To evaluate the integrity of genomic DNA in the hiPSCs, Comet assay was performed for ♂ARSA$^{mut/mut}$, ♀ARSA$^{wt/mut}$ and ♂ARSA$^{wt/mut}$. Results demonstrated variable degree of DNA damage between the individuals as indicated by tail intensity (Figure 4.7. A). The levels of DNA damage in ♀ARSA$^{wt/mut}$ was found to be significantly higher than ♂ARSA$^{mut/mut}$ and ♂ARSA$^{wt/mut}$ with p-values of $p < 0.05$ and $p < 0.0001$ respectively (Figure 4.7 B). Additionally, DNA damage in ♂ARSA$^{mut/mut}$ was observed to be significantly higher than ♂ARSA$^{wt/mut}$ with a p-value of $p < 0.01$. These findings indicate that while individual variability in DNA damage may exist, the overall levels of genomic instability are not directly related to the severity of *ARSA* genotype.

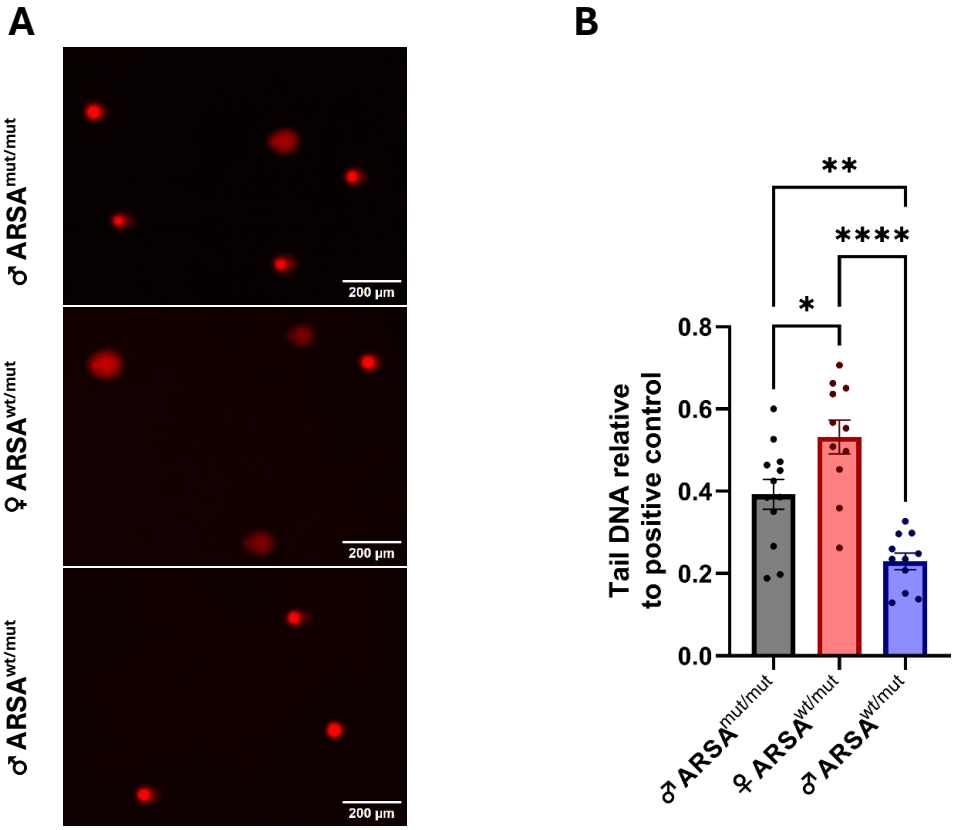

Figure 4.7. Comet assay analysis of DNA damage levels in hiPSCs.
A. Representative images from Comet assay in hiPSCs from ♂ARSA$^{mut/mut}$, ♀ARSA$^{wt/mut}$ and ♂ARSA$^{wt/mut}$. Scale bars = 200 µm **B.** Tail intensity values relative to positive control (HEK293T + H_2O_2). Each datapoint represents the mean tail intensity from one technical replicate. At least 40 cells were analyzed per replicate in six independent experiments per individual using ♂ARSA$^{mut/mut}$ (cl. 8.2, cl. 8.8 and cl. 8.9), ♀ARSA$^{wt/mut}$ (cl. 9.7 and 9.8) and ♂ARSA$^{wt/mut}$ (cl. 10.9 and 10.1). Error bars indicate mean ± SEM. Statistical significance between groups is noted by *$p < 0.05$, **$p \leq 0.01$, ****$p \leq 0.0001$, ns ≥ 0.05.

4.7. Neural differentiation of hiPSCs to O4+ oligodendrocytes

Given that the myelinating cells of the CNS are the primary affected cells in MLD (21, 35), it is beneficial to investigate the development of oligodendrocytes from hiPSCs derived from MLD-affected individuals. To test the potential of this approach, one fibroblast-derived hiPSC clone, originating from an MLD-diseased patient (subsection 3.1.1), was subjected to differentiation. Induction of SOX10 overexpression was conducted through viral transduction to promote the differentiation towards O4+ oligodendrocyte lineage, as proposed in the protocol by García-León et al. (81). The differentiation process is depicted across different morphological stages (Figure 4.8).

Cells were observed to develop into a more differentiated stage after inducing neural induction. At day 19, the cells demonstrated neural networks (Figure 4.8. D). Purification was performed to selectively isolate O4+ cells, resulting in pure culture of immature oligodendrocytes.

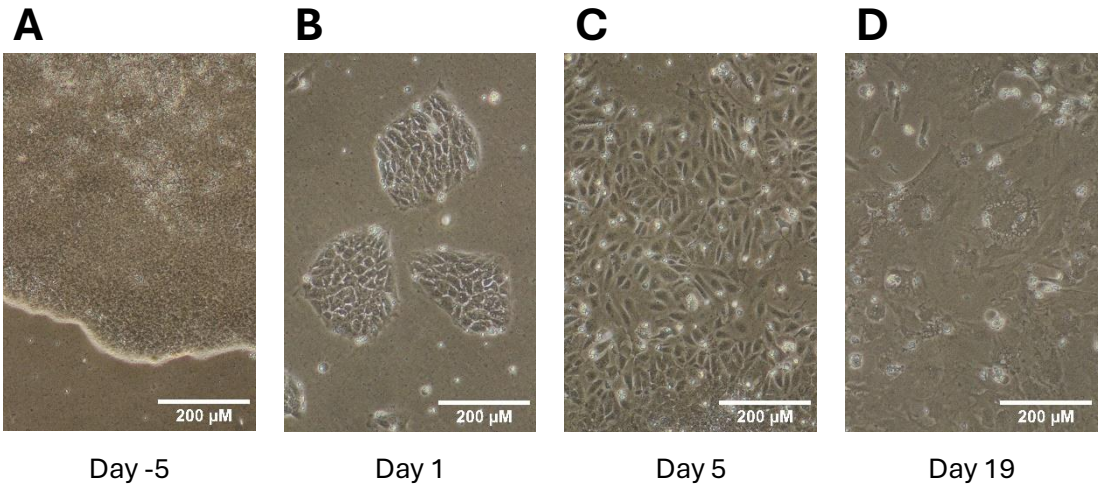

Figure 4.8. Neural differentiation of hiPSCs to O4+ oligodendrocytes.
Representative images depicting morphology of cells during different days of differentiation. Images from one trial of neural differentiation using fibroblast-derived hiPSCs originating from GM00243$^{mut/mut}$. **A.** hiPSC colony as basis for neural induction. **B.** Initiation of neural differentiation, day after changing to N2B27 medium. **C.** Differentiated cells two days prior to viral transduction. **D.** Cells 10 days post-viral transduction with SOX10 overexpression, showing early stages of oligodendrocyte development and formation of neural networks. Scale bars = 200 µm.

5. Discussion

MLD is a devastating disorder characterized by the accumulation of sulfatides in the CNS, leading to progressive demyelination and severe neurological outcomes (21). Despite its profound impact, the exact molecular and cellular mechanisms underlying MLD are not fully understood (21). This knowledge gap emphasizes the need for reliable models to study the disease pathophysiology. hiPSCs offer a promising way for such research, providing a relevant model to compare pathological processes in patients and healthy controls. In this project, hiPSCs derived from members of a family affected by MLD were utilized to establish a 2D cell culture model. This approach enabled the assessment and comparison of hiPSC characteristics and quality across individuals, including affected and unaffected family members.

5.1. Generation of hiPSCs and influencing factors

hiPSCs were generated from PBMCs for each individual of a family affected by MLD, consisting of a diseased child and carrier parents. The reprogramming process was successful across all samples. However, notable variations were observed in the resulting hiPSC lines. Specifically, the hiPSCs derived from ♂ARSA$^{wt/mut}$ displayed considerable challenges, including low cell attachment, heightened cell death rates, and an inclination for spontaneous differentiation. In contrast, hiPSC lines derived from the ♂ARSA$^{mut/mut}$ and ♀ARSA$^{wt/mut}$ exhibited greater stability and fewer phenotypic issues, where ♀ARSA$^{wt/mut}$ was observed to generate the most stable and reliable hiPSC clones. These discrepancies suggest that there are underlying factors that contribute to the observed variability in hiPSC reprogramming efficiency and stability.

Even when utilizing the same reprogramming methods, variability in iPSC generation has been observed to be significant, particularly in iPSCs derived from disease-specific patient lines (82). This variability is predominantly linked to the characteristics of the parental line intended for reprogramming, which is influenced by contributing factors such as method, efficiency of reprogramming and disease-specific mutations present in the donor cells (82, 83). Furthermore, the genetic background and epigenetic state of the donor cells are involved in determining the efficiency and quality of the resulting iPSCs

(84). Epigenetics involves the heritable traits in gene function that do not alter the DNA sequence itself, and play a fundamental role in regulating gene expression through mechanisms such as DNA methylation and histone modifications (84). The process of reprogramming differentiated cells to iPSCs involves a comprehensive reset of the epigenome, intended to erase somatic memory and reestablish a pluripotent state capable of differentiating into any cell type (84). However, the residual epigenetic memory from the original somatic cells and original gene expression profiles can influence this reset, leading to variations in the efficiency and quality of the resulting iPSCs (84, 85). Therefore, underlying genetic and epigenetic differences could be a contributing factor to the observed hiPSC differences from the different MLD-affected individuals in this thesis.

In addition to variable behavior and morphology of hiPSCs derived from the individuals, clonal variability was also observed. Previous studies have found significant intra-individual clonal variation in iPSCs, often surpassing the effect that originating tissue has on reprogramming efficiency (85, 86). The study by Kyttälä et al. found that iPSC lines retained donor-specific transcriptional signatures, implying that iPSCs from different donors express different sets of genes related to pluripotency and lineage specification (85). Additionally, donor-specific methylation patterns were present, affecting the gene expression and differentiation capacities in the iPSCs. These methylation differences persisted even after reprogramming, highlighting the influence of the donor's genetic background (85).

Due to the differences observed between the individuals, it would be advantageous to expand the sample size in future studies to include a greater number of donors. Incorporating broader genetic and epigenetic diversity would help mitigate the impact of individual-specific variations, thus enhancing the reliability and generalizability of the experimental outcomes. This would ensure that findings from subsequent experiments are more accurately attributed to the effects MLD, rather than being traits specific to individual genetic or epigenetic backgrounds.

5.2. Genome integrity and clonal variations in hiPSCs

In addition to previously existing genetic variations in donor cells, the process of reprogramming somatic cells to hiPSCs can result in the introduction of new mutations and copy number variants CNVs (87). These variants may occur due to the inherent stress of cellular reprogramming, which often leads to replication stress and genomic instability (87). Furthermore, genetic events during the long-term culture and expansion of hiPSCs are known to increase the probability of generating random mutations and new CNVs (88). Regular karyotyping can therefore be useful in detecting new chromosomal aberrations in the hiPSCs (88).

Karyotyping of the hiPSC clones derived from the three MLD-affected individuals demonstrated the detection of CNVs in selected clones, although without any single individual distinctly exhibiting a higher frequency or unique profile of these variants (Figure 4.2). This again highlights an inherent clonal variability. A significant proportion of somatic variants in iPSCs have been found to be subclonal, and have likely emerged during the early cell divisions following reprogramming (86). This results in a single iPSC line that can contain multiple subclones with distinct genetic profiles. This highlights the importance of using multiple iPSC clones in research, to ensure a broader genetic representation,

Expression of pluripotency and proliferation markers

The expression of pluripotency markers was assessed to evaluate the reprogramming efficiency and verify the maintenance of a stable pluripotent state in the hiPSCs. The assessment of pluripotency markers such as OCT4, SSEA4, SOX2, and NANOG provides essential insights into the cellular characteristics that dictate the utility of these hiPSC lines in subsequent experiments (54, 56). Through IF staining and RT-qPCR, the expression levels of these markers were examined across several individuals from different MLD-affected families.

First, IF analysis for MLD family 3 indicated no significant differences in the expression of OCT4 and SSEA4 among the individuals (Figure 4.3). This uniformity of the expression suggests that the hiPSC lines maintain a consistent pluripotent state, and that they are likely reliable for further experimental and therapeutic uses. Pluripotency

markers like OCT4 and SSEA4 are necessary for maintaining the self-renewal capabilities and undifferentiated state of stem cells and their uniform expression is a positive indicator of cell line quality and stability (54).

The RT-qPCR analysis further supports these findings. Here, the expression of the pluripotency markers OCT4, SOX2 and NANOG were analyzed among hiPSCs derived from MLD family 3, as well as two additional MLD-affected families. The results revealed generally comparable levels of pluripotency marker expression among the hiPSCs derived from all three families, albeit with some individual variation (Figure 4.6). This slight variability could again be attributed to inherent biological differences, variations in reprogramming efficiency, or minor discrepancies in culture conditions. However, the predominant similarity in pluripotency expression levels across the different families reinforces the robustness of the pluripotent state maintained in these hiPSCs.

In addition to assessing pluripotency markers, the expression of Ki67 was also examined across the hiPSC clones from the three individuals. Ki67 is a well-established marker of cell proliferation and is indicative of active cell cycling and growth potential of stem cell cultures (88). Notably, Ki67 expression was found to be comparable among the individuals within the MLD family 3 (Figure 4.5), suggesting that the cell proliferation rates are consistent across the hiPSC lines derived from different members of the family. The expression levels of Ki67 align with the findings from previous studies using MLD-derived iPSCs, where cell proliferation in both diseased- and healthy-derived iPSCs was found to be comparable (59).

DNA damage in hiPSCs

Assessment of DNA damage in the hiPSCs derived from the MLD family 3 was conducted using the Comet assay. This is a method for measuring DNA strand breaks in individual cells (89). Distinct variations in DNA damage were observed among the different family members. Specifically, ♂ARSA$^{wt/mut}$ exhibited the lowest levels of DNA damage and ♀ARSA$^{wt/mut}$ the highest levels (Figure 4.7).

It could be argued that the observed differences between the individual-derived hiPSCs in culture might be correlated to the variations in DNA damage. The ♀ARSA$^{wt/mut}$-

derived hiPSCs, despite showing the greatest DNA damage, were the most stable and showed the least differentiation tendency in culture. In contrast, ♂ARSA$^{wt/mut}$ gave rise to unstable clones, prone to cell death, low cell attachment and differentiation. Studies have underscored the tendency of iPSCs to harbor genomic abnormalities, which can be caused by the reprogramming process (90). Additionally, it has been documented that iPSCs possess a lower capacity for DNA damage repair compared to their embryonic stem cell counterparts and the original somatic cells from which they are derived (90). Therefore, observed DNA damage and quality in culture could be related to differences in the underlying molecular mechanisms of DNA repair and stress response among the hiPSCs derived from each individual.

When analyzing DNA damage within the hiPSCs, assessments were conducted separately for the male and female donors. DNA damage assessments revealed the highest levels in ♀ARSA$^{wt/mut}$ and the lowest in ♂ARSA$^{wt/mut}$. This discrepancy between the healthy controls may be attributable to gender differences. When excluding the impact of gender, and considering the results from both carrier parents together, DNA damage levels are observed to be comparable between ARSA$^{mut/mut}$ and ARSA$^{wt/mut}$. These findings could imply that gender could have an effect on the differences observed in the hiPSCs. Given that gender-specific biological differences are known to impact a range of cellular processes, including DNA repair mechanisms, stress responses, and metabolic activities, these factors could be significant in understanding the differing patterns of DNA damage observed in male and female-derived hiPSCs (91). Further studies should be conducted to investigate the impact of these factors.

ROS are byproducts of cellular metabolism that are particularly prevalent under pathological conditions, and are known to induce a broad spectrum of DNA damage, including single-strand breaks, double-strand breaks, and oxidative lesions (39, 46). Previous studies have reported increased ROS levels in MLD-derived hiPSCs compared to non-diseased counterparts (59). Results from the study by Frati et al. demonstrated elevated levels of ROS in hiPSCs derived from MLD patients (59). Findings from Frati et al. contrast the results from Comet assay in this study, as no significant differences in DNA damage levels were observed when comparing the MLD-affected child to the carrier parents (59). However, while the healthy control samples used in this study are carriers of MLD disease, they are not manifesting the disease themselves. This could imply that the cellular mechanisms compensating for the partial deficiency in ARSA

activity in carriers are sufficient to maintain lower levels of ROS, closer to those seen in completely healthy individuals without *ARSA* mutations (59). Therefore, the carrier status of the parents might not exhibit as pronounced differences in DNA damage compared to completely healthy donors, which could explain the lack of significant differences observed between the MLD-affected child and the carrier parents in this study.

Additionally, while DNA damage in hiPSCs can be influenced by elevated ROS levels, it is important to consider that other mechanisms may also contribute to genome instability (92). Elevated ROS levels do not necessarily translate directly to increased levels of DNA damage, and it could therefore be interesting to assess the level of ROS in the MLD-derived hiPSCs directly to obtain a clearer understanding of how the disease might affect DNA damage between individuals. Furthermore, including more individuals and families could enhance the reliability of the results and allow for a broader understanding of the genetic and environmental variability affecting ROS production and DNA damage. Due to time restraints, Comet assay was only performed for one of the MLD families. It would be interesting to examine other MLD families to verify the findings from this study.

5.3. Germ layer marker expression and differentiation potential

Under suitable culture conditions, iPSCs should have the ability to spontaneously differentiate into EBs, giving rise to cell types from all three germ layers: ectoderm, mesoderm, and endoderm (93, 94). The formation of EBs and the subsequent analysis of germ layer markers within these EBs are therefore critical steps for assessing the pluripotency and differentiation potential of the hiPSCs. Simultaneously, pluripotency markers are expected to decrease as differentiation is initiated (57, 94).

Notable variations in EB formation efficiency were observed across the different hiPSC lines. Additionally, inconsistencies were evident within the individual clones and across repeated experiments with the same clone (Figure 4.5 A). EBs have previously been described to exhibit significant variability in differentiation outcomes across different cell lines and cultures due to spontaneous formation, thus leading to inconsistent results even under controlled culture settings (93). The differentiation outcomes are significantly influenced by the quality of the EBs, such as cell number and size. The viability of EBs

and their success in achieving terminal differentiation are notably dependent on their size, as EBs that are too small tend to exhibit poor survival rates during differentiation, whereas overly large EBs are prone to core necrosis (93). Therefore, it is important to conduct multiple experiments from the hiPSC clones to ensure the reproducibility and reliability of differentiation outcomes.

Gene expression was assessed for the cells at hiPSC stage (Day 0) and at EB stage (Day 4). Germ layer marker analysis revealed varying levels of expression across the individuals, and between the distinct hiPSC clones (Figure 4.5 C-G). By reviewing the expression for each individual, a slight tendency towards increased mRNA levels at EB stage was observed for the markers. However, the considerable imbalance between the hiPSC clones questions the reliability of these results. Expression of pluripotency marker OCT4 was found to decrease across the hiPSCs during differentiation to EBs (Figure 4.5 B), indicating loss of pluripotency as the cells develop into a more differentiated state. For several of the germ layer markers, the ♂ARSA$^{wt/mut}$ genotype exhibits a slight elevation in expression levels at the hiPSC stage relative to other genotypes. Furthermore, this genotype demonstrates the least change in expression upon differentiation to EBs, which suggests a less pronounced differentiation potential. Notably, the hiPSCs from the ♂ARSA$^{wt/mut}$ genotype were more challenging to reprogram and subsequently exhibited difficulties in forming EBs, suggesting a hindered potential in transitioning from a pluripotent to a differentiated state. However, due to time constraints and difficulty in EB formation for certain clones, only one experiment was performed for two or three clones per individual. It would have been preferable to replicate this experiment to enhance the reliability of the results. Moreover, additional biological replicates would have been favorable if a greater yield of EBs could have been obtained.

Differentiation of hiPSCs to oligodendrocytes

Given the predominant role that oligodendrocytes have in demyelinating diseases such as MLD, the differentiation of hiPSCs to oligodendrocytes poses a valuable method for unraveling pathomechanisms of the disease (81). Due to the variable quality of the fibroblast-derived hiPSCs and time constraints, only one hiPSC line underwent differentiation to O4+ oligodendrocytes (Figure 4.8).

hiPSCs were initially induced to OLIG2+ OPCs and were further differentiated to O4+ immature oligodendrocytes by SOX10 induction. O4+ specific purification indicated the presence of O4+ oligodendrocytes in culture. However, further studies should be performed to confirm oligodendrocyte purity and expression of the O4 marker. IF analysis or RT-qPCR could be used to assess the expression of O4 and OLIG2 at the different stages of differentiation. Although further analyses were not conducted for this specific experiment, it demonstrates the potential of differentiating patient-specific hiPSCs to neural cells to investigate the effects of ARSA deficiency in neurodevelopment (59, 81).

6. Conclusions and Future Perspectives

The aim of this master thesis was to generate and characterize hiPSCs as a study model for MLD, and compare properties and markers between hiPSCs derived from MLD patients and those from healthy individuals. hiPSCs were successfully generated by reprogramming PBMCs from a family affected by MLD, consisting of a diseased child and healthy carrier parents of MLD.

Karyotyping analysis revealed the hiPSCs clones with the highest genomic integrity that were selected for further analysis. Assessment of pluripotency markers, OCT4, SSEA4, SOX2 and NANOG, and the proliferation marker Ki67 revealed uniform expression among the hiPSCs, indicating their stable pluripotent state and capability of subsequent directed differentiation. Comparable expression of pluripotency markers across individuals from two additional MLD-affected families further supported these findings. Nevertheless, notable differences in culturing efficiency and cell behavior were observed among the hiPSCs derived from the different donors, and between the distinct clones. Especially hiPSCs derived from ♂ARSA$^{wt/mut}$ exhibited challenges related to increased cell death and a higher tendency of spontaneous differentiation. Furthermore, EB formations and germ layer marker analysis demonstrated considerable variability across both genotypes and between individual clones, highlighting the influence of individual-derived differences on hiPSCs and subsequent differentiation potential. Moreover, significant variations in DNA damage levels were observed within the individuals, with the highest levels detected in the ♀ARSA$^{wt/mut}$ and the lowest in the ♂ARSA$^{wt/mut}$. Despite higher DNA damage, hiPSCs from the female carrier exhibited greater stability and a reduced tendency for differentiation. These findings suggest that factors beyond DNA integrity, such as gender-specific biological differences and individual variations in DNA repair mechanisms, likely influence hiPSC behavior and stability.

The conclusions drawn from this project are based on data collected from a limited number of clones, mainly originating from a single MLD-affected family. This drawback may limit the generalizability of the findings, as they could be influenced by individual-specific differences inherent to the subjects studied. Future studies should expand the sample size to include a broader selection of families and affected individuals. This will help to mitigate the impact of individual variability and provide a more comprehensive understanding of the cellular dynamics associated with MLD in hiPSCs.

Future studies should focus on the possibility of differentiating hiPSCs to neural cells, such as oligodendrocytes, to study MLD pathology. The potential to use these O4+ OPCs in co-culture systems with neurons is particularly valuable for simulating the myelination and demyelination process *in vitro* (81). Such models can be useful in dissecting the underlying molecular mechanisms of MLD, and have the potential to unveil novel therapeutic targets and pave the way for the development of new therapies for MLD.

References

1. Penati R, Fumagalli F, Calbi V, Bernardo ME, Aiuti A. Gene therapy for lysosomal storage disorders: recent advances for metachromatic leukodystrophy and mucopolysaccaridosis I. J Inherit Metab Dis. 2017;40(4):543-54.
2. Maegawa GHB. Lysosomal Leukodystrophies Lysosomal Storage Diseases Associated With White Matter Abnormalities. J Child Neurol. 2019;34(6):339-58.
3. Appelqvist H, Wäster P, Kågedal K, Öllinger K. The lysosome: from waste bag to potential therapeutic target. J Mol Cell Biol. 2013;5(4):214-26.
4. Simonaro CM. Lysosomes, Lysosomal Storage Diseases, and Inflammation. Journal of Inborn Errors of Metabolism and Screening. 2016;4:2326409816650465.
5. Rajkumar V, Dumpa V. Lysosomal Storage Disease. StatPearls. Treasure Island (FL): StatPearls Publishing

6. Luciani M, Gritti A, Meneghini V. Human iPSC-Based Models for the Development of Therapeutics Targeting Neurodegenerative Lysosomal Storage Diseases. Front Mol Biosci. 2020;7:224.
7. Borger DK, McMahon B, Roshan Lal T, Serra-Vinardell J, Aflaki E, Sidransky E. Induced pluripotent stem cell models of lysosomal storage disorders. Dis Model Mech. 2017;10(6):691-704.
8. AVROBIO. Patients and Families: Lysosomal Disorders 2024 [Available from: https://www.avrobio.com/patients-families/lysosomal-storage-disorders/.
9. Conway R. The Sphingolipidoses. In: Rubin IL, Merrick J, Greydanus DE, Patel DR, editors. Health Care for People with Intellectual and Developmental Disabilities across the Lifespan. Cham: Springer International Publishing; 2016. p. 659-82.
10. Nagpal R, Goyal RB, Priyadarshini K, Kashyap S, Sharma M, Sinha R, et al. Mucopolysaccharidosis: A broad review. Indian J Ophthalmol. 2022;70(7):2249-61.
11. Khan SA, Tomatsu SC. Mucolipidoses Overview: Past, Present, and Future. Int J Mol Sci. 2020;21(18).
12. Leslie N. BL. Pompe Disease. 2007 Updated November 2nd 2023 [cited April 28th 2024]. In: GeneReviews [Internet]. Seattle (WA): University of Washington, Seattle, [cited April 28th 2024]. Available from: https://www.ncbi.nlm.nih.gov/books/NBK1261/.
13. Kaur A, Dhaliwal AS, Raynes H, Naidich TP, Kaufman DM. Diagnosis and Supportive Management of Fucosidosis: A Case Report. Cureus. 2019;11(11):e6139.
14. Federico A, Palmeri S. Oligosaccharidoses. In: Hollak CEM, Lachmann R, editors. Inherited Metabolic Disease in Adults: A Clinical Guide: Oxford University Press; 2016. p. 0.
15. Michalski JC, Klein A. Glycoprotein lysosomal storage disorders: alpha- and beta-mannosidosis, fucosidosis and alpha-N-acetylgalactosaminidase deficiency. Biochim Biophys Acta. 1999;1455(2-3):69-84.
16. Wang RY, Bodamer OA, Watson MS, Wilcox WR. Lysosomal storage diseases: diagnostic confirmation and management of presymptomatic individuals. Genet Med. 2011;13(5):457-84.
17. van der Knaap MS, Bugiani M. Leukodystrophies: a proposed classification system based on pathological changes and pathogenetic mechanisms. Acta Neuropathol. 2017;134(3):351-82.

18. Ceravolo G, Zhelcheska K, Squadrito V, Pellerin D, Gitto E, Hartley L, et al. Update on leukodystrophies and developing trials. J Neurol. 2024;271(1):593-605.
19. Nowacki JC, Fields AM, Fu MM. Emerging cellular themes in leukodystrophies. Front Cell Dev Biol. 2022;10:902261.
20. van Rappard DF, Boelens JJ, Wolf NI. Metachromatic leukodystrophy: Disease spectrum and approaches for treatment. Best Pract Res Clin Endocrinol Metab. 2015;29(2):261-73.
21. Shaimardanova AA, Chulpanova DS, Solovyeva VV, Mullagulova AI, Kitaeva KV, Allegrucci C, et al. Metachromatic Leukodystrophy: Diagnosis, Modeling, and Treatment Approaches. Front Med (Lausanne). 2020;7:576221.
22. Biffi A. ARSA gene homepage - Global Variome shared LOVD 2010 [updated April 19, 2024. Available from: https://databases.lovd.nl/shared/genes/ARSA.
23. Filocamo M. The PSAP gene homepage - Global Variome shared LOVD 2013 [updated 2024 April 19. Available from: https://databases.lovd.nl/shared/genes/PSAP.
24. Cesani M, Lorioli L, Grossi S, Amico G, Fumagalli F, Spiga I, et al. Mutation Update of ARSA and PSAP Genes Causing Metachromatic Leukodystrophy. Hum Mutat. 2016;37(1):16-27.
25. Berger J, Löschl B, Bernheimer H, Lugowska A, Tylki-Szymanska A, Gieselmann V, et al. Occurrence, distribution, and phenotype of arylsulfatase A mutations in patients with metachromatic leukodystrophy. Am J Med Genet. 1997;69(3):335-40.
26. Beerepoot S, van Dooren SJM, Salomons GS, Boelens JJ, Jacobs EH, van der Knaap MS, et al. Metachromatic leukodystrophy genotypes in The Netherlands reveal novel pathogenic ARSA variants in non-Caucasian patients. Neurogenetics. 2020;21(4):289-99.
27. OrchardTherapeutics. Libmeldy - Indication: Orchard Therapeutics; 2023 [updated June 2023. Available from: https://www.libmeldy.eu/indication/.
28. Jonckheere AI, Kingma SDK, Eyskens F, Bordon V, Jansen AC. Metachromatic leukodystrophy: To screen or not to screen? Eur J Paediatr Neurol. 2023;46:1-7.
29. Gieselmann V, Krägeloh-Mann I. Metachromatic leukodystrophy--an update. Neuropediatrics. 2010;41(1):1-6.
30. Gomez-Ospina N. Arylsulfatase A Deficiency. In: Adam MP, Feldman J, Mirzaa GM, Pagon RA, Wallace SE, Bean LJH, et al., editors. GeneReviews(®). Seattle (WA): University of Washington, Seattle

31. Doherty K, Frazier SB, Clark M, Childers A, Pruthi S, Wenger DA, et al. A closer look at ARSA activity in a patient with metachromatic leukodystrophy. Mol Genet Metab Rep. 2019;19:100460.
32. Barrell C. Juvenile metachromatic leukodystrophy: understanding the disease and implications for nursing care. J Pediatr Oncol Nurs. 2007;24(2):64-9.
33. van Rappard DF, de Vries ALC, Oostrom KJ, Boelens JJ, Hollak CEM, van der Knaap MS, et al. Slowly Progressive Psychiatric Symptoms: Think Metachromatic Leukodystrophy. J Am Acad Child Adolesc Psychiatry. 2018;57(2):74-6.
34. Köhler W, Curiel J, Vanderver A. Adulthood leukodystrophies. Nat Rev Neurol. 2018;14(2):94-105.
35. Eckhardt M. The role and metabolism of sulfatide in the nervous system. Mol Neurobiol. 2008;37(2-3):93-103.

36. Blomqvist M, Zetterberg H, Blennow K, Månsson JE. Sulfatide in health and disease. The evaluation of sulfatide in cerebrospinal fluid as a possible biomarker for neurodegeneration. Mol Cell Neurosci. 2021;116:103670.
37. Moyano AL, Li G, Lopez-Rosas A, Månsson JE, van Breemen RB, Givogri MI. Distribution of C16:0, C18:0, C24:1, and C24:0 sulfatides in central nervous system lipid rafts by quantitative ultra-high-pressure liquid chromatography tandem mass spectrometry. Anal Biochem. 2014;467:31-9.
38. Farah MH, Dali C, Groeschel S, Moldovan M, Whiteman DAH, Malanga CJ, et al. Effects of sulfatide on peripheral nerves in metachromatic leukodystrophy. Ann Clin Transl Neurol. 2024;11(2):328-41.
39. Kuhn S, Gritti L, Crooks D, Dombrowski Y. Oligodendrocytes in Development, Myelin Generation and Beyond. Cells. 2019;8(11).
40. Barateiro A, Brites D, Fernandes A. Oligodendrocyte Development and Myelination in Neurodevelopment: Molecular Mechanisms in Health and Disease. Curr Pharm Des. 2016;22(6):656-79.
41. Miller RH, Mi S. Dissecting demyelination. Nat Neurosci. 2007;10(11):1351-4.
42. Czepiel M, Boddeke E, Copray S. Human oligodendrocytes in remyelination research. Glia. 2015;63(4):513-30.
43. Dali C, Barton NW, Farah MH, Moldovan M, Månsson JE, Nair N, et al. Sulfatide levels correlate with severity of neuropathy in metachromatic leukodystrophy. Ann Clin Transl Neurol. 2015;2(5):518-33.
44. Gieselmann V. Metachromatic leukodystrophy: genetics, pathogenesis and therapeutic options. Acta Paediatr. 2008;97(457):15-21.
45. Miller RH, Fyffe-Maricich S, Caprariello AC. Animal models for the study of multiple sclerosis. Animal models for the study of human disease: Elsevier; 2017. p. 967-88.
46. Cooke MS, Evans MD, Dizdaroglu M, Lunec J. Oxidative DNA damage: mechanisms, mutation, and disease. Faseb j. 2003;17(10):1195-214.
47. Thibert KA, Raymond GV, Tolar J, Miller WP, Orchard PJ, Lund TC. Cerebral Spinal Fluid levels of Cytokines are elevated in Patients with Metachromatic Leukodystrophy. Sci Rep. 2016;6:24579.
48. Laudanna C, Constantin G, Baron P, Scarpini E, Scarlato G, Cabrini G, et al. Sulfatides trigger increase of cytosolic free calcium and enhanced expression of tumor necrosis factor-alpha and interleukin-8 mRNA in human neutrophils. Evidence for a role of L-selectin as a signaling molecule. J Biol Chem. 1994;269(6):4021-6.
49. d'Azzo A, Tessitore A, Sano R. Gangliosides as apoptotic signals in ER stress response. Cell Death & Differentiation. 2006;13(3):404-14.
50. Beerepoot S, Nierkens S, Boelens JJ, Lindemans C, Bugiani M, Wolf NI. Peripheral neuropathy in metachromatic leukodystrophy: current status and future perspective. Orphanet J Rare Dis. 2019;14(1):240.
51. Bergner CG, van der Meer F, Winkler A, Wrzos C, Türkmen M, Valizada E, et al. Microglia damage precedes major myelin breakdown in X-linked adrenoleukodystrophy and metachromatic leukodystrophy. Glia. 2019;67(6):1196-209.
52. Hess B, Saftig P, Hartmann D, Coenen R, Lüllmann-Rauch R, Goebel HH, et al. Phenotype of arylsulfatase A-deficient mice: relationship to human metachromatic leukodystrophy. Proc Natl Acad Sci U S A. 1996;93(25):14821-6.
53. Ramakrishnan H, Hedayati KK, Lüllmann-Rauch R, Wessig C, Fewou SN, Maier H, et al. Increasing sulfatide synthesis in myelin-forming cells of arylsulfatase A-deficient mice

causes demyelination and neurological symptoms reminiscent of human metachromatic leukodystrophy. J Neurosci. 2007;27(35):9482-90.
54. Ye L, Swingen C, Zhang J. Induced pluripotent stem cells and their potential for basic and clinical sciences. Curr Cardiol Rev. 2013;9(1):63-72.
55. Du P, Wu J. Hallmarks of totipotent and pluripotent stem cell states. Cell Stem Cell. 2024.
56. Zhao W, Ji X, Zhang F, Li L, Ma L. Embryonic Stem Cell Markers. Molecules. 2012;17(6):6196-236.
57. Guo NN, Liu LP, Zheng YW, Li YM. Inducing human induced pluripotent stem cell differentiation through embryoid bodies: A practical and stable approach. World J Stem Cells. 2020;12(1):25-34.
58. Kiecker C, Bates T, Bell E. Molecular specification of germ layers in vertebrate embryos. Cell Mol Life Sci. 2016;73(5):923-47.
59. Frati G, Luciani M, Meneghini V, De Cicco S, Ståhlman M, Blomqvist M, et al. Human iPSC-based models highlight defective glial and neuronal differentiation from neural progenitor cells in metachromatic leukodystrophy. Cell Death Dis. 2018;9(6):698.
60. Doerr J, Böckenhoff A, Ewald B, Ladewig J, Eckhardt M, Gieselmann V, et al. Arylsulfatase A Overexpressing Human iPSC-derived Neural Cells Reduce CNS Sulfatide Storage in a Mouse Model of Metachromatic Leukodystrophy. Mol Ther. 2015;23(9):1519-31.
61. De Vitis E, Stanzione A, Romano A, Quattrini A, Gigli G, Moroni L, et al. The Evolution of Technology-Driven In Vitro Models for Neurodegenerative Diseases. Adv Sci (Weinh). 2024;11(16):e2304989.
62. Wray S. Modelling neurodegenerative disease using brain organoids. Semin Cell Dev Biol. 2021;111:60-6.
63. Sreenivasamurthy S, Laul M, Zhao N, Kim T, Zhu D. Current progress of cerebral organoids for modeling Alzheimer's disease origins and mechanisms. Bioeng Transl Med. 2023;8(2):e10378.
64. Singh N, Singh AK. In Silico Structural Modeling and Binding Site Analysis of Cerebroside Sulfotransferase (CST): A Therapeutic Target for Developing Substrate Reduction Therapy for Metachromatic Leukodystrophy. ACS Omega. 2024;9(9):10748-68.
65. Esmail S, Danter WR. Artificially Induced Pluripotent Stem Cell-Derived Whole-Brain Organoid for Modelling the Pathophysiology of Metachromatic Leukodystrophy and Drug Repurposing. Biomedicines. 2021;9(4).
66. Fumagalli F, Calbi V, Natali Sora MG, Sessa M, Baldoli C, Rancoita PMV, et al. Lentiviral haematopoietic stem-cell gene therapy for early-onset metachromatic leukodystrophy: long-term results from a non-randomised, open-label, phase 1/2 trial and expanded access. Lancet. 2022;399(10322):372-83.
67. Sanchez-Alvarez NT, Bautista-Niño PK, Trejos-Suárez J, Serrano-Diaz NC. Metachromatic leukodystrophy: diagnosis and treatment challenges. Bionature. 2021;3:2083-90.
68. Armstrong N, Olaye A, Noake C, Pang F. A systematic review of clinical effectiveness and safety for historical and current treatment options for metachromatic leukodystrophy in children, including atidarsagene autotemcel. Orphanet J Rare Dis. 2023;18(1):248.
69. Messina M, Gissen P. Atidarsagene autotemcel for metachromatic leukodystrophy. Drugs Today (Barc). 2023;59(2):63-70.
70. C ÍD, Groeschel S, Moldovan M, Farah MH, Krägeloh-Mann I, Wasilewski M, et al. Intravenous arylsulfatase A in metachromatic leukodystrophy: a phase 1/2 study. Ann Clin Transl Neurol. 2021;8(1):66-80.

71. Matzner U, Herbst E, Hedayati KK, Lüllmann-Rauch R, Wessig C, Schröder S, et al. Enzyme replacement improves nervous system pathology and function in a mouse model for metachromatic leukodystrophy. Hum Mol Genet. 2005;14(9):1139-52.
72. Stroobants S, Gerlach D, Matthes F, Hartmann D, Fogh J, Gieselmann V, et al. Intracerebroventricular enzyme infusion corrects central nervous system pathology and dysfunction in a mouse model of metachromatic leukodystrophy. Hum Mol Genet. 2011;20(14):2760-9.
73. Wolf NI, Breur M, Plug B, Beerepoot S, Westerveld ASR, van Rappard DF, et al. Metachromatic leukodystrophy and transplantation: remyelination, no cross-correction. Ann Clin Transl Neurol. 2020;7(2):169-80.
74. Rosenberg JB, Kaminsky SM, Aubourg P, Crystal RG, Sondhi D. Gene therapy for metachromatic leukodystrophy. J Neurosci Res. 2016;94(11):1169-79.
75. Boucher AA, Miller W, Shanley R, Ziegler R, Lund T, Raymond G, et al. Long-term outcomes after allogeneic hematopoietic stem cell transplantation for metachromatic leukodystrophy: the largest single-institution cohort report. Orphanet J Rare Dis. 2015;10:94.
76. Biffi A, De Palma M, Quattrini A, Del Carro U, Amadio S, Visigalli I, et al. Correction of metachromatic leukodystrophy in the mouse model by transplantation of genetically modified hematopoietic stem cells. J Clin Invest. 2004;113(8):1118-29.
77. Sessa M, Lorioli L, Fumagalli F, Acquati S, Redaelli D, Baldoli C, et al. Lentiviral haemopoietic stem-cell gene therapy in early-onset metachromatic leukodystrophy: an ad-hoc analysis of a non-randomised, open-label, phase 1/2 trial. Lancet. 2016;388(10043):476-87.
78. Beslutningsforum. Beslutningsforum 19. juni: Libmeldy-genterapi til barn, Trodelvy-brystkreftmedisin og Crohns-legemiddel innføres: Nye Metoder; 2023 [Available from: https://www.nyemetoder.no/se/aktuelt/beslutningsforum-19-juni-libmeldy-genterapi-til-barn-trodelvy-brystkreftmedisin-og-crohns-legemiddel-innfores/.
79. Hossain MA, Hasegawa-Ogawa M, Manome Y, Igarashi M, Wu C, Suzuki K, et al. Generation and characterization of motor neuron progenitors and motor neurons using metachromatic leukodystrophy-induced pluripotent stem cells. Mol Genet Metab Rep. 2022;31:100852.
80. Lund RJ, Nikula T, Rahkonen N, Närvä E, Baker D, Harrison N, et al. High-throughput karyotyping of human pluripotent stem cells. Stem Cell Res. 2012;9(3):192-5.
81. García-León JA, García-Díaz B, Eggermont K, Cáceres-Palomo L, Neyrinck K, Madeiro da Costa R, et al. Generation of oligodendrocytes and establishment of an all-human myelinating platform from human pluripotent stem cells. Nat Protoc. 2020;15(11):3716-44.
82. Malik N, Rao MS. A review of the methods for human iPSC derivation. Methods Mol Biol. 2013;997:23-33.
83. Martins-Taylor K, Xu RH. Concise review: Genomic stability of human induced pluripotent stem cells. Stem Cells. 2012;30(1):22-7.
84. Haridhasapavalan KK, Raina K, Dey C, Adhikari P, Thummer RP. An Insight into Reprogramming Barriers to iPSC Generation. Stem Cell Reviews and Reports. 2020;16(1):56-81.
85. Kyttälä A, Moraghebi R, Valensisi C, Kettunen J, Andrus C, Pasumarthy KK, et al. Genetic Variability Overrides the Impact of Parental Cell Type and Determines iPSC Differentiation Potential. Stem Cell Reports. 2016;6(2):200-12.
86. Volpato V, Webber C. Addressing variability in iPSC-derived models of human disease: guidelines to promote reproducibility. Dis Model Mech. 2020;13(1).
87. Liang G, Zhang Y. Genetic and epigenetic variations in iPSCs: potential causes and implications for application. Cell Stem Cell. 2013;13(2):149-59.

88. Uxa S, Castillo-Binder P, Kohler R, Stangner K, Müller GA, Engeland K. Ki-67 gene expression. Cell Death & Differentiation. 2021;28(12):3357-70.
89. Olive PL, Banáth JP. The comet assay: a method to measure DNA damage in individual cells. Nature Protocols. 2006;1(1):23-9.
90. Zhang M, Yang C, Liu H, Sun Y. Induced pluripotent stem cells are sensitive to DNA damage. Genomics Proteomics Bioinformatics. 2013;11(5):320-6.
91. Kiris E. Human-Induced Pluripotent Stem Cell-Based Models for Studying Sex-Specific Differences in Neurodegenerative Diseases. Adv Exp Med Biol. 2022;1387:57-88.
92. Yoshihara M, Hayashizaki Y, Murakawa Y. Genomic Instability of iPSCs: Challenges Towards Their Clinical Applications. Stem Cell Rev Rep. 2017;13(1):7-16.
93. Pettinato G, Wen X, Zhang N. Formation of well-defined embryoid bodies from dissociated human induced pluripotent stem cells using microfabricated cell-repellent microwell arrays. Sci Rep. 2014;4:7402.
94. Lin Y, Chen G. Embryoid body formation from human pluripotent stem cells in chemically defined E8 media. StemBook. Cambridge (MA): Harvard Stem Cell Institute

Appendix

Table A.1. Serum-free expansion medium composition.

Reagent (final concentration)	Producer, Catalogue nr.
StemSpan H300	StemCell Technologies, 1000-0073
Human recombinant stem cell factor (SCF) (100 ng/ml)	R&D Systems, 255-SC-050
Human IL3 Recombinant protein (10 ng/ml)	Gibco, PHC0035
Human recombinant Erythropoietin (EPO) (3 U/ml)	R&D Systems, 287-TC-500
Human IGF-1 (40 ng/ml)	Miltenyi Biotec, 130-093-886
Dexamethasone (1 µM)	Sigma-Aldrich, D4902

Table A.2. Human induced pluripotent stem cell (hiPSC) medium composition.

Reagent (final concentration)	Producer, Catalogue nr.
Advanced DMEM (Reduced serum media)	Gibco, 12491023
KnockOut Serum Replacement (10%)	Gibco, 10828028
L-glutamine (2 mM)	Gibco, 25030081
2-Mercaptoethanol (5 µM)	Gibco, 31350-010
Recombinant Human bFGF (4 ng/ml)	PeproTech, 100-18B
Penicillin-Streptomycin (1%)	Gibco, 15140122

Table A.3. Embryoid bodies (EBs) medium composition.

Reagent (final concentration)	Producer, Catalogue nr.
DMEM/F-12, HEPES	Gibco, 11330032
Penicillin-Streptomycin (1%)	Gibco, 15140122
KnockOut Serum Replacement (20%)	Gibco, 10828028
GlutaMAX Supplement (1X)	Gibco, 35050061
MEM Non-Essential Amino Acids Solution (1X)	Gibco, 11140050
2-Mercaptoethanol (100 µM)	Gibco, 31350010

Table A.4. List of forward and reverse primers used for RT-qPCR (5' to 3' direction).

Marker	Forward sequence	Reverse sequence	Producer
BMP4	ATCAAACTAGCATGGCTCGC	TGGCTGTCAAGAATCATGGA	Sigma
FOXC1	TGTTCGAGTCACAGAGGATCG	ACAGTCGTAGACGAAAGCTCC	Sigma
GATA4	GTGTCCCAGACGTTCTCAGTC	GGGAGACGCATAGCCTTGT	Sigma
NANOG	AATACCTCAGCCTCCAGCAGATG	CTGCGTCACACCATTGCTATTCT	Sigma
NESTIN	GGCGCACCTCAAGATGTCC	CTTGGGGTCCTGAAAGCTG	Sigma
OCT4	TCAGGAGATATGCAAAGCAGAAAC	CTGATCTGCTGCAGTGTGGG	Sigma
PAX6	GCCCTCACAAACACCTACAG	TCATAACTCCGCCCATTCAC	Sigma
SOX17	CGCTTTCATGGTGTGGGCTAAGGACG	TAGTTGGGGTGGTCCTGCATGTGCTG	Sigma
SOX2	GCCGAGTGGAAACTTTTGTCG	GGCAGCGTGTACTTATCCTTCT	Sigma

Table A.5. Primary and secondary antibodies used for immunofluorescence (IF) analysis.

Primary Antibody	Isotype	Dilution	Producer, Catalogue nr.
anti-Oct-4A (C30A3) Rabbit mAb	Rabbit IgG	1:200	Cell Signaling, 2840
anti-SSEA4 (MC813) Mouse mAb	Mouse IgG3	1:200	Cell Signaling, 4755
anti-Ki67	Rabbit IgG	1:500	Abcam, ab15580

Secondary Antibody	Dilution	Producer, Catalogue nr.
Alexa Fluor 594 goat anti-rabbit	1:500	Thermo Fisher, A11037
Alexa Fluor 488 donkey anti-mouse	1:500	Thermo Fisher, A21202

Table A.6. EVOS microscope settings for immunofluorescence (IF) analysis and Comet assay

Analysis	Target	EVOS light cube	Objective
Pluripotency markers (subsection)	DAPI OCT4 SSEA4	tgBFP TexasRed GFP	10X
Proliferation (subsection)	DAPI Ki67	tgBFP TexasRed	10X
Comet Assay (subsection)	SYBR Green	YFP	10X

Table A.7. N2B27 medium composition

Reagent (final concentration)	Producer, Catalogue nr
DMEM/F-12, HEPES	Gibco, 11330032
Penicillin-Streptomycin (1%)	Gibco, 15140122
MEM Non-Essential Amino Acids Solution (1X)	Gibco, 11140050
2-Mercaptoethanol (100 µM)	Gibco, 31350010
N-2 Supplement (1X)	Gibco, 17502001
B-27 Supplement (1X)	Gibco, 12587010
Insulin (25 µg/ml)	Sigma-Aldrich. I9278

Table A.8. Oligodendrocyte differentiation medium composition

Reagent (final concentration)	Producer, Catalogue nr.
N2B27 medium	
Recombinant Human PDGF-AA (10 ng/ml)	PeproTech, 100-13A
Recombinant Human IGF-1 (10 ng/ml)	Miltenyi Biotec 130-093-886
Recombinant Human HGF (5 ng/ml)	PeproTech, 100-39H
Recombinant Human NT-3 (10 ng/ml)	PeproTech, 450-03
Biotin (100 ng/ml)	Sigma-Aldrich, B4639
Cyclic adenosine monophosphate (cAMP) (1µM)	Merck, D0627
3,3′,5-Triiodo-L-thyronine (60 ng/ml)	Sigma-Aldrich, T2877
Doxycycline hyclate (1µg/ml)	Merck, D9891

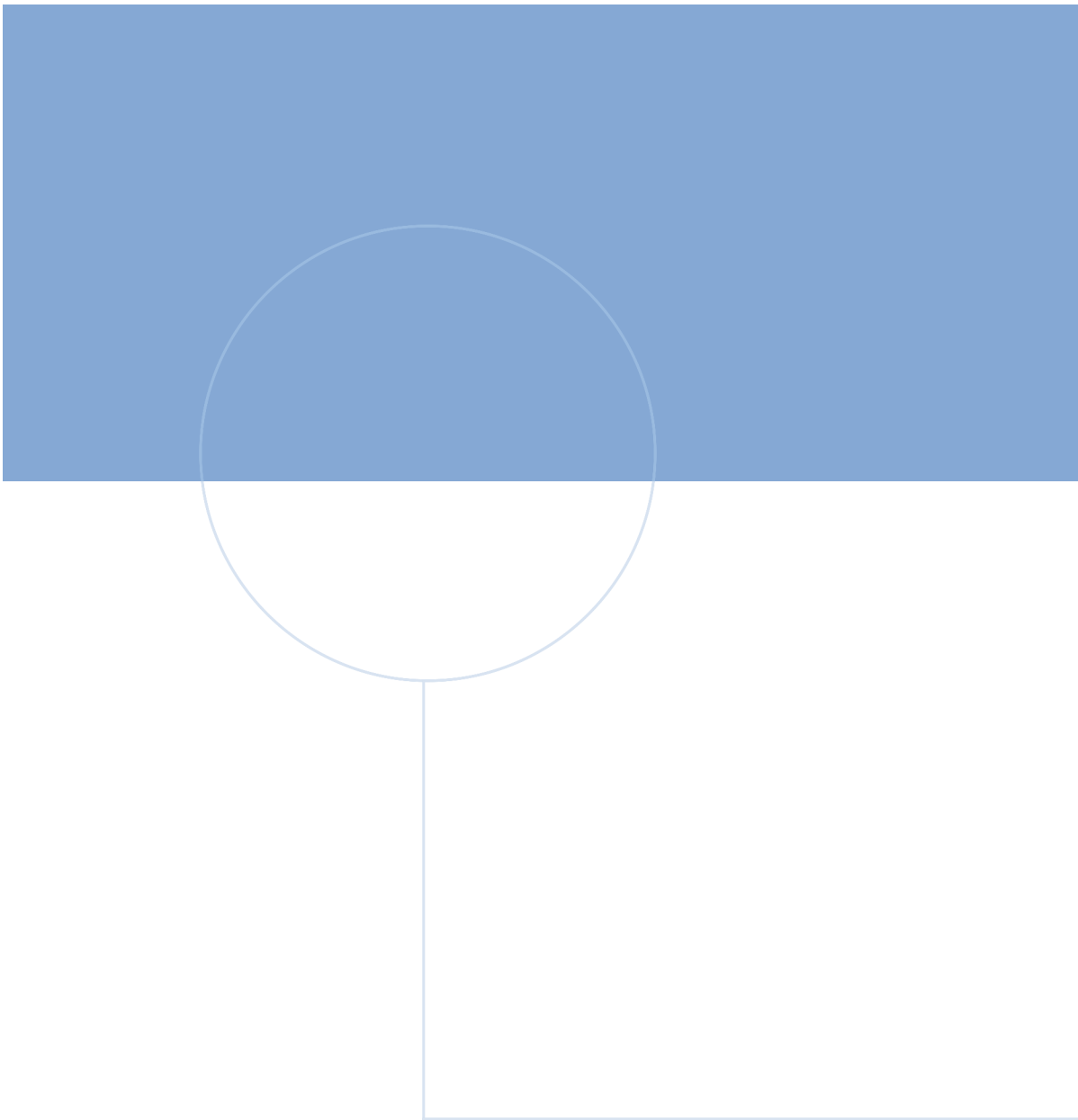

NTNU

Norwegian University of
Science and Technology